Article

Immunity

Roquin Suppresses the PI3K-mTOR Signaling Pathway to Inhibit T Helper Cell Differentiation and Conversion of Treg to Tfr Cells

Graphical Abstract

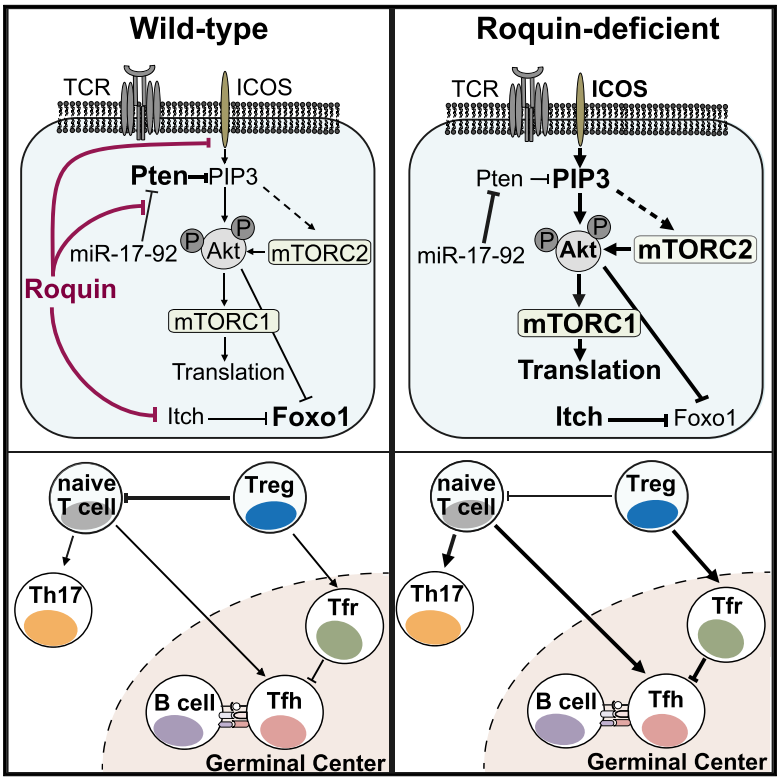

Highlights

- Roquin deficiency in Treg cells impairs suppression of conventional T cells
- Treg cells lacking Roquin upregulate Tfh cell genes and specialize to Tfr cells
- Roquin represses PI3K-mTOR and Akt signaling in Treg and CD4$^+$ T cells
- Inhibition of PI3K-mTOR corrects differentiation of Roquin-deficient CD4$^+$ T cells

Authors

Katharina Essig, Desheng Hu, Joao C. Guimaraes, ..., Mihaela Zavolan, Dirk Baumjohann, Vigo Heissmeyer

Correspondence

desheng_hu@126.com (D.H.), vigo.heissmeyer@med.uni-muenchen.de (V.H.)

In Brief

Essig et al. show that spontaneous activation and aberrant differentiation of Roquin-deficient T cells involves cell-intrinsic causes in not only conventional T cells but also impaired Treg cell function. In both cell types, Roquin inhibits the PI3K-mTOR signaling pathway at several levels, thereby controlling protein biosynthesis and limiting differentiation toward Th17 and Tfh cells as well as preventing the conversion and functional specialization of Treg into Tfr cells.

Essig et al., 2017, Immunity *47*, 1067–1082
December 19, 2017 © 2017 Elsevier Inc.
https://doi.org/10.1016/j.immuni.2017.11.008

CellPress

Please cite this article in press as: Essig et al., Roquin Suppresses the PI3K-mTOR Signaling Pathway to Inhibit T Helper Cell Differentiation and Conversion of Treg to Tfr Cells, Immunity (2017), https://doi.org/10.1016/j.immuni.2017.11.008

CellPress

Roquin Suppresses the PI3K-mTOR Signaling Pathway to Inhibit T Helper Cell Differentiation and Conversion of Treg to Tfr Cells

Katharina Essig,[1,9] Desheng Hu,[1,9,10,*] Joao C. Guimaraes,[2] Dominik Alterauge,[1] Stephanie Edelmann,[3] Timsse Raj,[1] Jan Kranich,[1] Gesine Behrens,[1] Alexander Heiseke,[1] Stefan Floess,[4] Juliane Klein,[1] Andreas Maiser,[5] Susan Marschall,[6] Martin Hrabě de Angelis,[6] Heinrich Leonhardt,[5] Cornelis F. Calkhoven,[7] Elfriede Noessner,[8] Thomas Brocker,[1] Jochen Huehn,[4] Anne B. Krug,[1] Mihaela Zavolan,[2] Dirk Baumjohann,[1] and Vigo Heissmeyer[1,3,*]

[1]Institute for Immunology, Biomedical Center, Ludwig-Maximilians-Universität München, 82152 Planegg-Martinsried, Germany
[2]Computational and Systems Biology, Biozentrum, University of Basel, 4056 Basel, Switzerland
[3]Research Unit Molecular Immune Regulation, Helmholtz Zentrum München, 81377 München, Germany
[4]Experimental Immunology, Helmholtz Centre for Infection Research, 38124 Braunschweig, Germany
[5]Center for Integrated Protein Science, Department of Biology, Ludwig-Maximilians-Universität München, 82152 Planegg-Martinsried, Germany
[6]German Center for Diabetes Research (DZD), 85764 Neuherberg, German Mouse Clinic, Institute of Experimental Genetics, Helmholtz Zentrum München, German Research Center for Environmental Health, 85764 Neuherberg, Chair of Experimental Genetics, School of Life Science Weihenstephan, Technische Universität München, Freising 85353, Germany
[7]European Research Institute for the Biology of Ageing (ERIBA), University Medical Center Groningen, University of Groningen, 9700 AD Groningen, the Netherlands
[8]Immunoanalytics Core Facility, Helmholtz Zentrum München, 81377 München, Germany
[9]These authors contributed equally
[10]Present address: Department of Integrated Traditional Chinese and Western Medicine, Union Hospital, Tongji Medical College, Huazhong University of Science and Technology, 430022 Wuhan, China
*Correspondence: desheng_hu@126.com (D.H.), vigo.heissmeyer@med.uni-muenchen.de (V.H.)
https://doi.org/10.1016/j.immuni.2017.11.008

SUMMARY

Roquin proteins preclude spontaneous T cell activation and aberrant differentiation of T follicular helper (Tfh) or T helper 17 (Th17) cells. Here we showed that deletion of Roquin-encoding alleles specifically in regulatory T (Treg) cells also caused the activation of conventional T cells. Roquin-deficient Treg cells downregulated CD25, acquired a follicular Treg (Tfr) cell phenotype, and suppressed germinal center reactions but could not protect from colitis. Roquin inhibited the PI3K-mTOR signaling pathway by upregulation of *Pten* through interfering with miR-17∼92 binding to an overlapping *cis*-element in the *Pten* 3′ UTR, and downregulated the Foxo1-specific E3 ubiquitin ligase Itch. Loss of Roquin enhanced Akt-mTOR signaling and protein synthesis, whereas inhibition of PI3K or mTOR in Roquin-deficient T cells corrected enhanced Tfh and Th17 or reduced iTreg cell differentiation. Thereby, Roquin-mediated control of PI3K-mTOR signaling prevents autoimmunity by restraining activation and differentiation of conventional T cells and specialization of Treg cells.

INTRODUCTION

Roquin-1 and Roquin-2 redundantly inhibit spontaneous T cell activation and CD4$^+$ T cell differentiation (Bertossi et al., 2011; Jeltsch et al., 2014; Vinuesa et al., 2005; Vogel et al., 2013). Consistently, mice with a homozygous *sanroque* missense mutation in the Roquin-1-encoding gene *Rc3h1* develop T follicular helper (Tfh) cell-driven lupus-like autoimmunity (Vinuesa et al., 2005). Moreover, combined deletion of the Roquin-encoding genes *Rc3h1* and *Rc3h2* in T cells causes Tfh and T helper 17 (Th17) cell accumulation and inflammation-associated pathology in the lung (Jeltsch et al., 2014; Vogel et al., 2013). Roquins are RNA-binding proteins that recognize specific stem-loop structures in 3′ UTRs of target mRNAs (Janowski et al., 2016; Leppek et al., 2013). Their targets include the mRNAs of costimulatory receptors *Icos*, *Ctla4*, and *Ox40*, cytokines *Tnf* and *Il6*, transcription factors *Irf4* and *cRel*, and modulators of transcription *Nfkbid* and *Nfkbiz* (Jeltsch and Heissmeyer, 2016). The T cell-expressed targets as well as the T cell receptor (TCR)-dependent regulation by the paracaspase MALT1 (Gewies et al., 2014; Jeltsch et al., 2014) may explain the prominent role of Roquin proteins in T cells and in the prevention of autoimmune and auto-inflammatory responses (Jeltsch and Heissmeyer, 2016), despite their ubiquitous expression.

Spontaneous activation of T cells and accumulation of Tfh cells also occur following miR17∼92 cluster overexpression and upon deletion of one *Pten* allele in lymphocytes (Baumjohann et al., 2013a; Kang et al., 2013; Xiao et al., 2008). The lipid phosphatase Pten dephosphorylates phosphatidylinositol-3,4,5-tris-phosphate (PIP3), counteracting the activity of the lipid kinase PI3K (Rolf et al., 2010). Downstream of PI3K is the mammalian target of rapamycin (mTOR) that integrates environmental cues from growth factors, nutrients, and cytokines to induce metabolic changes. mTOR is present in two distinct complexes, mTORC1 and mTORC2, which are characterized by their

regulatory proteins Raptor and Rictor, respectively (Pollizzi and Powell, 2015). mTOR controls cellular protein synthesis by regulating the translation apparatus.

PIP3 production by T cells is positively correlated with the magnitude of immunization-induced germinal center (GC) formation (Rolf et al., 2010). The underlying Tfh cell differentiation requires signaling through mTORC1 and mTORC2 (Yang et al., 2016b; Zeng et al., 2016), and Tfh cell-dependent GC formation is controlled by a specialized subset of follicular regulatory T (Tfr) cells (Chung et al., 2011; Linterman et al., 2011; Wollenberg et al., 2011). Activation-induced miRNAs from the miR-17∼92 cluster repress Pten, which explains the antagonistic effects of miR-17∼92 and Pten on Tfh cell formation (Baumjohann et al., 2013a; Kang et al., 2013; Xiao et al., 2008). Pten also has a critical role in Treg cells, as *Pten*-deficient Treg cells lose CD25 expression as well as the ability to control the spontaneous activation of conventional T cells, and to prevent Tfh cell accumulation and autoimmunity (Huynh et al., 2015; Shrestha et al., 2015).

In T cells, PI3K activity is strongly induced by ICOS signaling and inactivates Foxo1, which interferes with Tfh and Th17 cell differentiation but promotes the function of Treg cells (Kerdiles et al., 2010; Lainé et al., 2015; Stone et al., 2015). Connected to PI3K signaling are mTORC1 and mTORC2 complexes, which, through so-far unknown downstream targets, enable Th17, Th2, Tfh, and Treg cell differentiation (Delgoffe et al., 2009, 2011; Kurebayashi et al., 2012; Lee et al., 2010; Sauer et al., 2008; Zeng et al., 2016).

The mechanisms of spontaneous activation and aberrant differentiation of Roquin-deficient T cells has not been defined yet. Here we uncover that Roquin inhibits the PI3K-mTOR pathway at several levels, thereby controlling protein biosynthesis, inhibiting differentiation toward Th17 and Tfh cells and conversion of Treg into Tfr cells.

RESULTS

Roquin Expression Is Required for Treg Cell Function

To investigate the role of Roquin-mediated post-transcriptional gene regulation in Treg cells, we combined a transgene for Treg cell-specific Cre recombinase expression from the *Foxp3* locus (*Foxp3-IRES-YFP-Cre*) (Rubtsov et al., 2008) with floxed alleles encoding Roquin-1 and Roquin-2 (*Rc3h1*$^{fl/fl}$; *Rc3h2*$^{fl/fl}$) to generate *Rc3h1*$^{fl/fl}$; *Rc3h2*$^{fl/fl}$; *Foxp3-IRES-YFP-Cre* (DKO^{Treg}) mice. Targeted exons were efficiently deleted in Treg cells (CD4$^+$YFP$^+$) of these mice (Figure 1A). The frequencies and numbers of Treg cells (Foxp3$^+$CD4$^+$) were normal in the thymus but were strongly increased in the spleen and to a lesser extent in peripheral lymph nodes (Figures 1B–1D). DKO^{Treg} mice shared the splenomegaly of mice that lacked Roquin expression in peripheral T cells due to *Cd4-Cre*-mediated deletion (DKO^T) (Figures S1A–S1C) but not other phenotypes such as the increase in CD8$^+$ or decrease in CD4$^+$ T and B220$^+$ B cell frequencies (Figures S1D–S1F). Older (3–4 months) DKO^{Treg} mice appeared healthy but showed a pronounced effector-memory phenotype (CD62L$^-$CD44$^+$) in CD4$^+$YFP$^+$ Treg cells as well as in CD4$^+$YFP$^-$ and CD8$^+$ conventional T cells (Figure 1E). Compared to age- and sex-matched WT controls, older DKO^{Treg} mice also exhibited increased frequencies and numbers of PD1^{int}CXCR5^{int}CD4$^+$ Tfh cells in the CD4$^+$, the non-Treg (CD4$^+$YFP$^-$) and Treg cell (CD4$^+$YFP$^+$) fractions (Figure S1G), while the observed increase in PD1^{hi}CXCR5^{hi}CD4$^+$ GC Tfh cells within the CD4$^+$ fraction was solely due to increased Tfr cell frequencies and numbers (Figures 1F and 1G). Compared to wild-type, DKO^{Treg} mice had increased IgM and IgG and significantly higher IgG1 levels in the sera (Figure S1H).

Among the PD1^{hi}CXCR5^{hi}CD4$^+$ T cells, the Tfr to GC Tfh cell ratio was strongly shifted toward the Tfr cell subset (Figures 2A and 2B). In female DKO^{Treg} mice harboring only one *Foxp3-IRES-YFP-Cre* allele, Roquin-deficient YFP$^+$Foxp3$^+$ Treg cells outnumbered YFP$^-$Foxp3$^+$ (WT) Treg cells (Figure 2C) and in the YFP$^+$ Treg cells the proportion of Tfr cells was strongly increased (Figures 2C and 2D). These data suggest that under homeostatic conditions, Roquin-deficient Treg cells expand, adopt a Tfr cell phenotype, and cannot suppress activation of conventional CD4$^+$ and CD8$^+$ T cells.

Roquin-Deficient Tfr Cells Repress Antigen-Specific B Cell Responses

To assess the functionality of Roquin-deficient Tfr cells, we immunized DKO^{Treg} mice with sheep red blood cells (SRBCs). The spleens of these mice had significantly smaller GCs compared to immunized control mice (Figures 2E and 2F) but more CD4$^+$Foxp3$^+$ cells per GC and GC area (Figure 2F). We also asked how the increased abundance of Tfr cells in DKO^{Treg} mice affected antibody titers and affinity maturation after immunization with the T cell-dependent antigen NP-KLH (Figures 2G–2M). Relative to wild-type controls, immunized DKO^{Treg} mice showed increased Tfr cell frequencies and numbers, no change for Tfh cells, while GC B cell numbers increased 1 week after immunization (Figures S1I and S1J). However, frequencies and numbers of NP-specific GC B cells 1 week after immunization were strongly decreased (Figures 2G–2I). Whereas IgG1 levels were elevated (Figure 2J), the generation of NP-specific IgG1 antibodies was impaired (Figures 2K and 2L), and DKO^{Treg} mice also showed reduced affinity maturation compared to WT mice (Figure 2M). These data reveal that Roquin-deficient Tfr cells are more abundant in the GCs and are functional in repressing antigen-specific B cell responses and antibody maturation efficiently.

Roquin-Deficient Treg Cells Are Less Protective in the B Cell-Independent Colitis Model

We next tested the suppressive activity of Roquin-deficient and WT Treg cells in the absence of B cells (Figures 3 and S2). Co-culture of different ratios of Treg cells with conventional CD4$^+$ T cells labeled with a proliferation dye revealed that WT and Roquin-deficient Treg cells similarly inhibited conventional CD4$^+$ T cells proliferation (Figure S2A). However, the Roquin-deficient Treg cell to conventional CD4$^+$ T cell ratio increased compared to samples with WT Treg cells (Figure S2B), which could mask a partial functional impairment. Next we compared the ability of Roquin-deficient and WT CD4$^+$YFP$^+$ Treg cells to protect from T cell transfer-induced colitis (Figures 3A–3E and S2C–S2E). *Rag1*$^{-/-}$ mice injected with naive T cells and WT Treg cells gained body weight and showed no pathology in colon histology (Figures 3A–3C). In contrast, the transfer of naive CD4$^+$ T cells alone or together with Roquin-deficient Treg

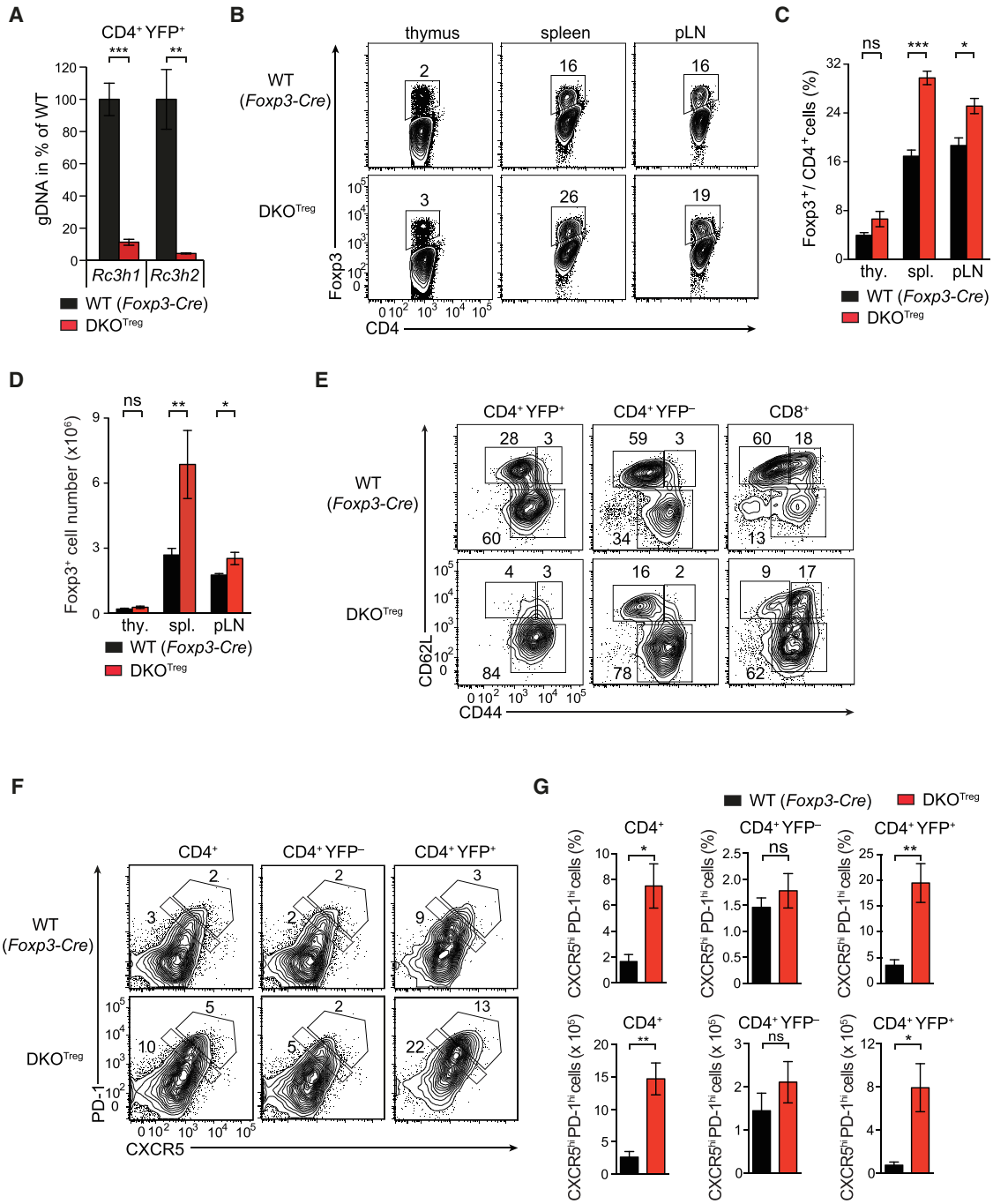

Figure 1. Altered Immune Homeostasis in Mice with Inactivation of Roquin in Treg Cells

(A) qPCR of *Rc3h1* and *Rc3h2* in genomic DNA (gDNA) of sorted CD4$^+$YFP$^+$ Treg cells from spleens of WT or DKO^{Treg} mice, normalized to WT.

(B–G) Flow cytometry of Foxp3 (B) CD62L and CD44 (E) or PD-1 and CXCR5 expression (F) performed on CD4$^+$ T cells (B, F) or CD4$^+$YFP$^+$, CD4$^+$YFP$^-$, and CD8$^+$ T cells from WT and DKO^{Treg} mice are displayed for the indicated organs (B) or spleens (E, F) of WT and DKO^{Treg} mice. For the analysis in (B), cellular frequencies and numbers are depicted in (C) and (D), respectively, or shown in (G) (upper and lower) for the analysis in (F).

Data are representative of four independent experiments with three mice (A) or one mouse (F, G) per group or six independent experiments with one mouse per group (B–E). Statistical significance was calculated by unpaired, two-tailed Student's t test *p < 0.05, **p < 0.01, and ***p < 0.001. Data are mean ± SEM.

cells caused colitis, significantly attenuated the weight gain of recipient mice (Figures 3A–3C), and caused the infiltration of leukocytes and CD3$^+$ T cells in the colon (Figure S2C). Furthermore, among infiltrating CD4$^+$ T cells, those which produced only IFN-γ as well as those with enhanced pathogenic potential, producing IL-17A and IFN-γ upon restimulation, were reduced in recipients of naive CD4$^+$ T cells and WT Treg cells compared to both other groups (Figure 3D). Although the frequencies of transferred WT

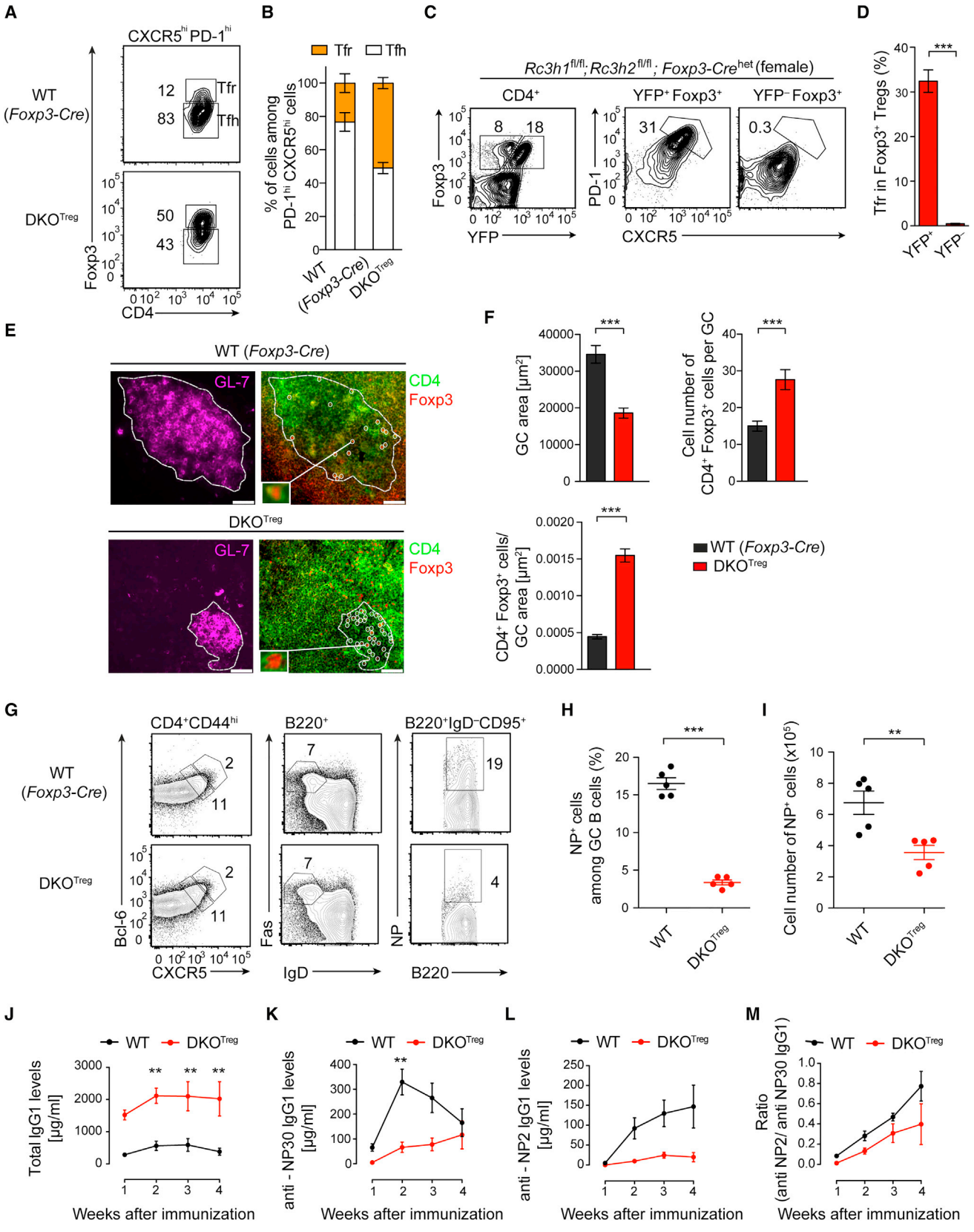

(legend on next page)

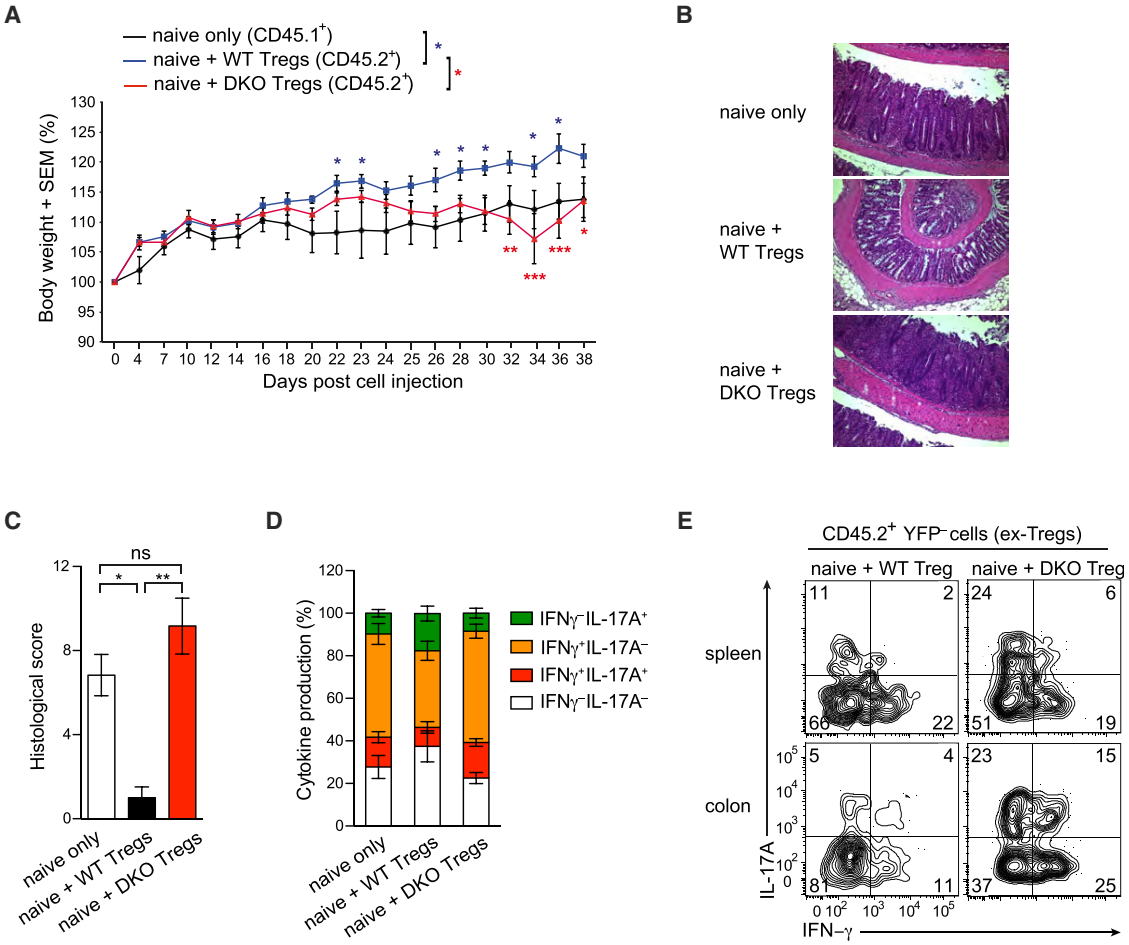

Figure 3. Roquin-Deficient Treg Cells Are Impaired to Protect from Colitis

Six *Rag1*$^{-/-}$ mice per group were injected with either CD4$^+$CD25$^-$CD44$^-$CD62L$^+$ cells from Ly5.1 mice alone or mixed with CD4$^+$YFP$^+$ Treg cells sorted from WT or DKO^{Treg} mice at a 2:1 ratio (naive:Treg cells). Post injection body weights were normalized to body weights on the day of injection (A). Bars indicate mean ± SEM. Statistical significance calculated for each time point was tested separately by two-way ANOVA with Tukey's multiple comparison test; *p < 0.05, **p < 0.01, and ***p < 0.001. After 38 days, the mice were sacrificed and half of the colon tissue was analyzed by histology (B and C). Data are presented as mean ± SEM (C), *p < 0.05 and **p < 0.01; ns, not significant (one-way ANOVA). The other half of the colon was analyzed by flow cytometry. Transferred CD45.1$^+$ cells (D) or CD45.2$^+$YFP$^-$ (ex-Treg) cells (E) were analyzed for cytokine expression after *ex vivo* stimulation. Bars indicate mean ± SEM (C and D).

and Roquin-deficient Treg cells (CD45.2$^+$CD4$^+$) were similar in the recipients' spleens (Figure S2D), Roquin-deficient Treg cells were less frequent among the CD4$^+$ T cells infiltrating the colon (Figure S2D). The transferred Roquin-deficient and WT Treg cells exhibited similar rates of loss in YFP or Foxp3 expression in the spleen or colon (Figure S2E, and data not shown). However, Roquin-deficient Treg cells (CD45.2$^+$CD4$^+$) from the colon that lost YFP expression (ex-Treg cells) were much more likely to produce IL-17A or IFN-γ or both upon *ex vivo* stimulation (Figure 3E). Finally, although the localization of Roquin-deficient Treg cells

Figure 2. Roquin-Deficient Treg Cells Suppress Antigen-Induced B Cell Responses

(A–D) Flow cytometry of Foxp3 expression in CD4$^+$CXCR5^{hi}PD-1^{hi} cells of splenic T cells from WT and DKO^{Treg} mice (A) or PD-1 and CXCR5 expression in splenic CD4$^+$YFP$^+$Foxp3$^+$ and YFP$^-$Foxp3$^+$ Treg cells from a heterozygous female DKO^{Treg} mouse (D). Frequencies of cells in (A) or (C) are shown in (B) or (D), respectively.

(E and F) Immunofluorescence of GL-7 (magenta), CD4 (green), and Foxp3 (red) in spleen sections from SRBC-immunized WT and DKO^{Treg} mice (scale bars, 50 μm) (E), with quantification of GC area and numbers of CD4$^+$Foxp3$^+$ cells per GC, or per μm^2 of GC area shown in (F).

(G) Flow cytometry of Tfh (left), GC B (middle), and NP-specific GC B (right) cells in the spleen of WT and DKO^{Treg} mice 7 days after immunization with NP-KLH, with frequencies (H) and numbers (I) of NP-specific GC B cells.

(J–M) Concentrations of total IgG1 (J), low-affinity NP30-recognizing (K), as well as high-affinity NP2-recognizing (L) NP-specific IgG1 antibodies in sera from NP-KLH immunized WT and DKO^{Treg} mice. Ratio of anti-NP2/anti-NP-30-specific IgG1 was determined for each time point as a measure of affinity maturation (M).

Data are representative of four independent experiments with one mouse per group (A, B), three independent experiments with one mouse per group (C, D), or one experiment with four (E, F), five (G–I), or six (J–M) mice per group. Statistical significance was calculated by unpaired, two-tailed Student's t test (A–I) or one-way ANOVA analysis with a Bonferroni post hoc test (J–M); **p < 0.01 and ***p < 0.001. Data are mean ± SEM.

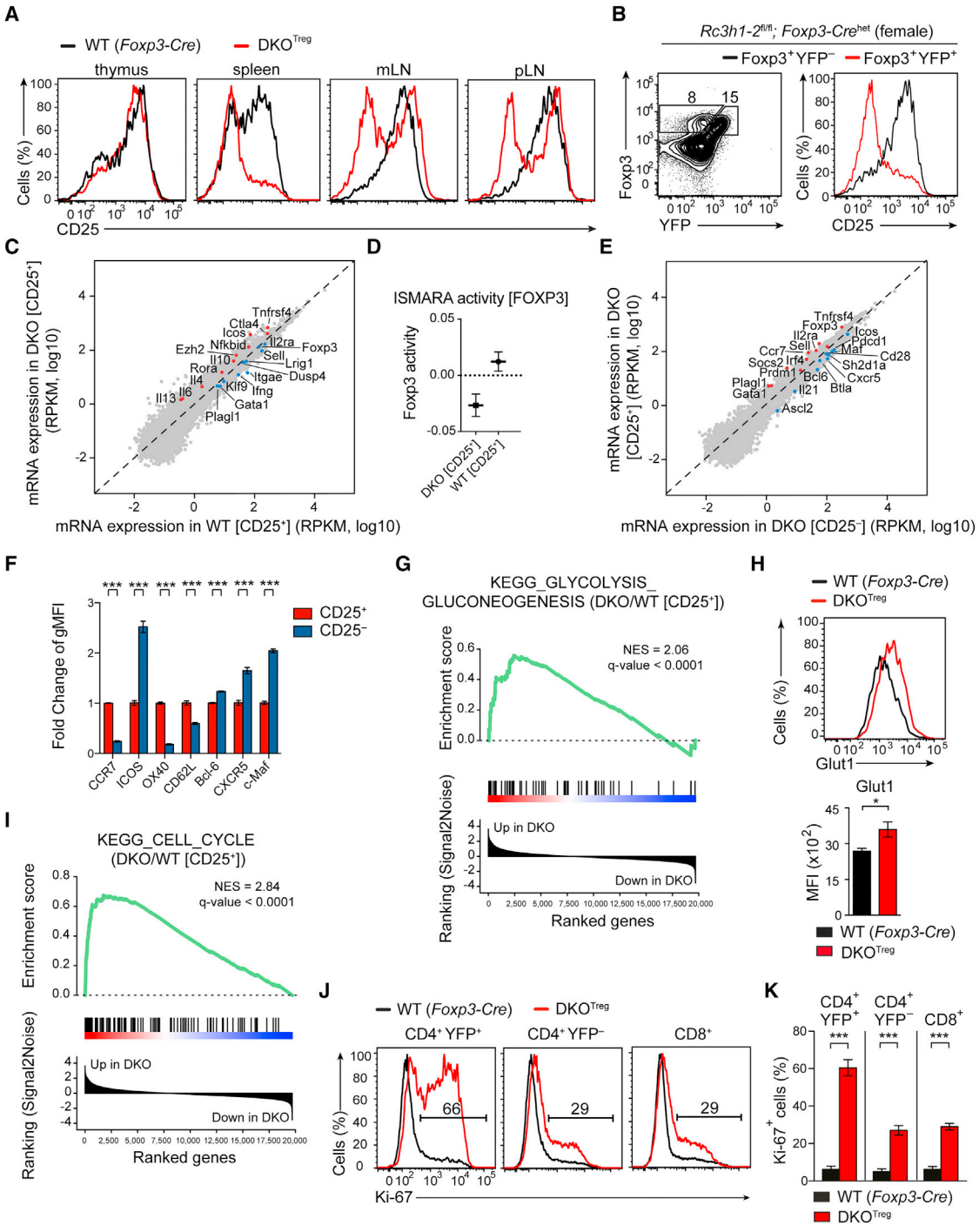

Figure 4. CD25 Downregulation on Roquin-Deficient Treg Cells Marks Tfr Cell Differentiation

(A and B) Expression of CD25 on CD4$^+$YFP$^+$ Treg cells (A) of the indicated organs from WT and DKO^{Treg} mice or on Foxp3$^+$YFP$^+$ and Foxp3$^+$YFP$^-$ cells from a female DKO^{Treg} mouse with heterozygous *IRES-YFP-Cre* expression (B).

(C and E) Gene expression profile of CD25$^+$ Treg cells from DKO^{Treg} or WT mice (C) or of CD25$^+$ compared to CD25$^-$ Treg cells from DKO^{Treg} mice (E).

(D) Inferred Foxp3 motif activity in CD25$^+$ Treg cells in DKO^{Treg} and WT mice. Error bars denote standard deviations of the inferred activities.

(F) Fold change of geometric mean fluorescence intensity (gMFI) of indicated markers comparing CD25$^+$ with CD25$^-$ Treg cells from DKO^{Treg} mice as shown in Figure S4F.

(G and I) Gene set enrichment analysis (GSEA) comparing the relative expression of genes in CD25$^+$ Treg cells in DKO^{Treg} mice compared to that of WT mice and examining the distribution of genes involved in glycolysis/gluconeogenesis (G) or cell cycle (I) as defined in the KEGG database (shown as black bars in the middle panel).

(legend continued on next page)

to the colon was not impaired (Figures S2F and S2G), these cells expressed significantly less CD103 (Figures S2I and S2J) and showed a propensity to downregulate Foxp3 protein expression while maintaining YFP levels (Figure S2H). Together, these data show that Roquin-deficient Treg cells are less protective in the adoptive T cell transfer colitis model.

Roquin-Deficient Treg Cells Lose CD25 Expression and Acquire a Tfh Cell Gene Signature

We next characterized the gene expression in Roquin-deficient Treg cells, which strongly downregulated CD25 expression (Figure 4A) but maintained high expression of Neuropilin-1 and Helios, two markers of thymus-derived Treg cells, and only slightly upregulated expression of CD122 and GITR (Figure S3A). CD25 downregulation was most pronounced in the spleen, less pronounced in lymph nodes, and not detectable in Foxp3^{+}YFP^{+} CD4SP thymocytes (Figure 4A). It occurred in a cell-intrinsic manner because female DKO^{Treg} mice with one *Foxp3-IRES-YFP-Cre* allele downregulated CD25 only in the YFP^{+} Treg cells (Figure 4B). Purified peripheral Treg cells that did or did not express CD25 displayed similar deletion of Roquin-encoding alleles (Figure S3B). However, *ex vivo* IL-2-stimulated Roquin-deficient CD4^{+}YFP^{+}CD25^{+} Treg cells showed an increased loss of Foxp3 and CD25 expression compared to WT counterparts (Figures S3C and S3D). Therefore, we investigated the impact of Roquin deficiency on the epigenetic fixation of the Treg cell phenotype by bisulfite sequencing (Floess et al., 2007). Using genomic DNA from thymic CD25^{+}YFP^{+}, splenic CD25^{+}YFP^{+}, and splenic CD25^{-}YFP^{+} Treg cells with or without Roquin, we did not detect differences in the TSDR methylation status in the *Foxp3* locus (Figure S3E). Roquin-deficient splenic CD25^{-} Treg cells proliferated stronger than the CD25^{+} counterparts as indicated by Ki-67 expression (Figure S3F).

To investigate the molecular basis of the Treg cell phenotype, we performed mRNA sequencing on sorted CD4^{+}YFP^{+}GITR^{+} CD25^{+} and CD4^{+}YFP^{+}GITR^{+}CD25^{-} cells from DKO^{Treg} and WT mice. When compared to WT counterparts, we found that many Roquin target genes including *IL6*, *Nfkbid*, *Icos*, *Ctla4*, and *Tnfrsf4* were upregulated in CD25-expressing Treg cells from DKO^{Treg} mice, as were the epigenetic regulator *Ezh2* and the Th17 cell-specific transcription factor *Rora* (Figure 4C). The mRNA abundance of cytokines such as *IL4* and *IL13* was increased, while *Ifng* was downregulated (Figure 4C). Cytokine expression was profoundly deregulated in supernatants of *ex vivo* stimulated Roquin-deficient Treg cells or conventional CD4^{+} T cells isolated from DKO^{Treg} mice, and in the sera of DKO^{Treg} compared to wild-type mice (Figures S4A–S4E). This suggests that gene regulation by Roquin in Treg cells not only controls functional plasticity of cytokine expression in these cells, but also has systemic consequences.

Among the mRNAs that are downregulated in CD25-expressing Treg cells from DKO^{Treg} mice, we found many that are commonly associated with a Treg cell signature, including *Foxp3*, *Il2ra*, *Plagl1*, *Lrig1*, *Klf9*, *Gata1*, *Itgae*, and *Dusp4* (Figure 4C; Haxhinasto et al., 2008). This was consistent with the decreased activity of the Foxp3 transcription factor inferred with ISMARA from the mRNA sequencing data (Figure 4D; Balwierz et al., 2014). Comparing gene expression in CD25^{+} and CD25^{-} Roquin-deficient Treg cells, the Treg cell signature genes segregated with CD25^{+} cells, while the Tfh signature genes, including *Sh2d1a*, *Maf*, *Bcl6*, *IL21*, *Pdcd1*, *Cxcr5*, and *Icos*, segregated with the CD25^{-} subset (Figure 4E). Flow cytometric analyses confirmed these expression differences between CD25^{+} and CD25^{-} subsets at the protein level (Figures 4F and S4F). Segregation of Tfh and Treg cell signatures was also present though less pronounced in CD25^{-} and CD25^{+} Treg cells from wild-type controls (compare Figures 4E and 4F and Figure S4G).

A similar downregulation of Treg cell signature genes has been reported to occur upon expression of a constitutively active form of the PIP3-induced kinase Akt (Haxhinasto et al., 2008). Conversely, expanded Treg cells and Tfr cells that lose CD25 expression and are unable to control activation of conventional T cells have been observed upon Treg cell-specific deletion of *Pten*, the negative regulator of PIP3 signaling (Huynh et al., 2015; Shrestha et al., 2015). These findings revealed an overlap of phenotypes between mice lacking Pten or Roquin in Treg cells (Huynh et al., 2015; Shrestha et al., 2015). *Pten*-deficient Treg cells showed an increased expression of mRNAs related to gene ontology of glycolysis and cell cycle (Shrestha et al., 2015), as we observed in DKO relative to WT CD25-expressing Treg cells (Figures 4G–4I). We further confirmed the increased surface expression of the glucose transporter Glut1 in Roquin-deficient Treg cells (Figure 4H). Consistent with proliferating Treg cells being impaired in their suppressive capacity (Gerriets et al., 2016), we found that Roquin-deficient Treg cells had increased proliferation (Figures 4J and 4K), while the fraction of Ki-67^{+} conventional CD4^{+} and CD8^{+} T cells was increased in the spleen of DKO^{Treg} mice (Figures 4J and 4K). Thus, Roquin deficiency impairs the expression of Treg cell signature genes, alters the metabolic activity and proliferative capacity of Treg cells, and induces Tfh cell-specific markers, indicating an imposed conversion to the Tfr cell subset.

Roquin Inhibits PI3K-mTOR Signaling

We therefore focused our investigation on cellular phenotypes that are expected consequences of increased PI3K-mTOR signaling. mTOR stimulates the translation of mRNAs of ribosomal proteins (RPs) and translation elongation factors that carry 5′ terminal oligopyrimidine (5′ TOP) motifs in their 5′ UTRs, thereby stimulating protein synthesis (Hsieh et al., 2012; Thoreen et al., 2012). In mRNA sequencing and ribosome footprint data from CD4^{+} T cells stimulated with PMA/ionomycin for 60 min, the inhibition of Roquin proteolysis by mepazine (Jeltsch et al., 2014) decreased the translation efficiency (TE) of 5′ TOP mRNAs and RP-encoding mRNAs relative to all others (Figure 5A). Also, Roquin inactivation and Roquin-1 overexpression in MEF cells led to consistent results (Figures S5A and S5B), and metabolic

(H, J, and K) Flow cytometry and quantification of Glut1 or Ki-67 expression in the indicated T cell subsets from spleens of WT and DKO^{Treg} mice.
Data are representative of six independent experiments with one mouse per group (A, B), one experiment with five WT and seven DKO^{Treg} mice (C–E, G, I), one experiment with four mice per group (F, H), or four independent experiments with one mouse per group (J, K). Statistical significance was calculated by unpaired, two-tailed Student's t test; *$p < 0.05$ and ***$p < 0.001$. Data are mean ± SEM.

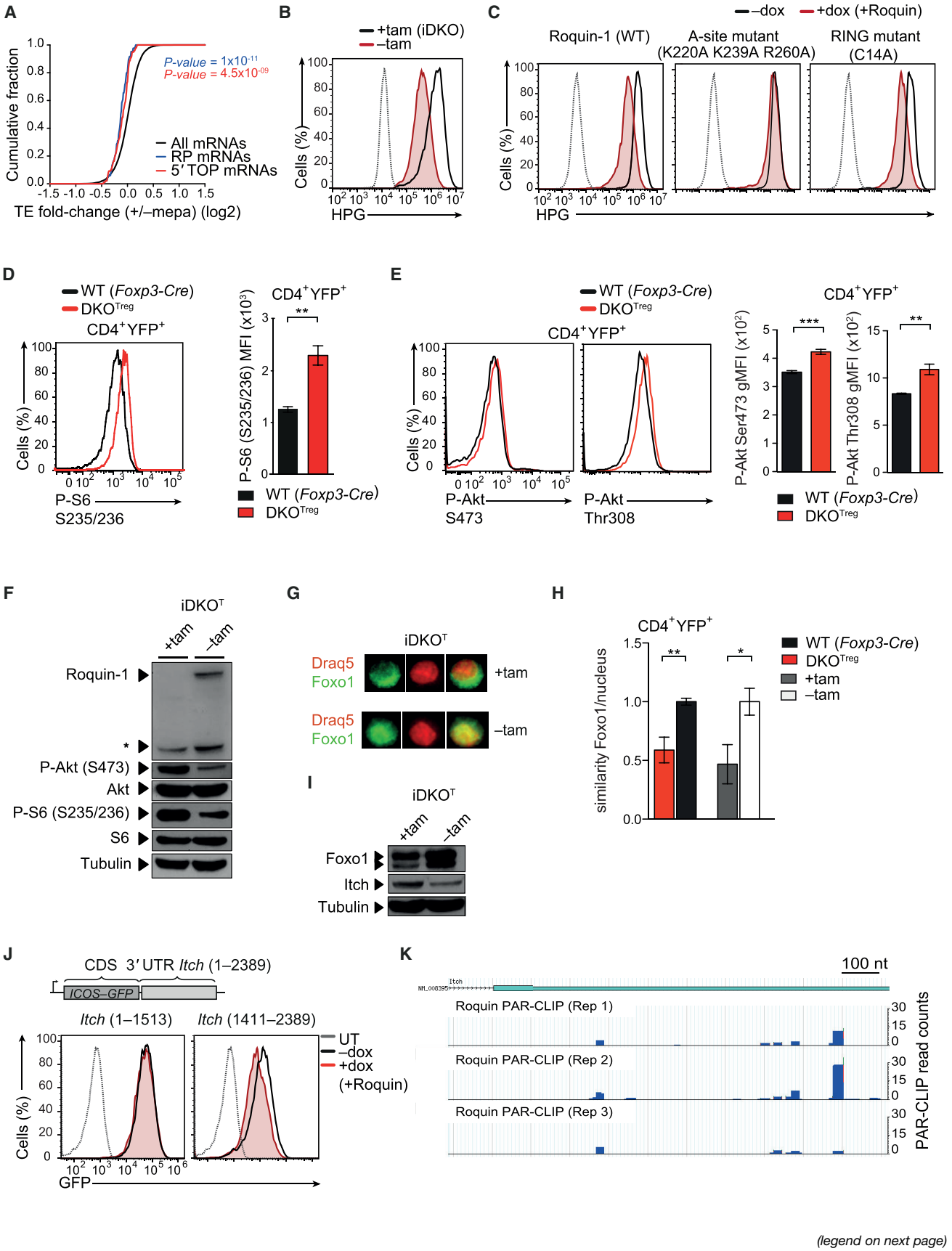

(legend on next page)

labeling of MEF cells with the fluorescence-tagged methionine analog L-homopropargylglycine (HPG) showed that induced deletion of Roquin caused increased incorporation of HPG and thereby promoted protein synthesis (Figure 5B).

Contrary to suggestions that Roquin impinges on mTORC1 signaling by negatively regulating the 5′ adenosine monophosphate-activated protein kinase α (AMPKα) through its RING finger (Ramiscal et al., 2015), we here found that the RING finger of Roquin-1 was not required for Roquin-mediated inhibition of protein synthesis (Figures 5C and S5D). However, we confirmed a partially impaired aggregation of the Roquin-1 RING finger mutant in stress granules (Figure S5E) and normal localization in P bodies (Figure S5F; Ramiscal et al., 2015). With different Roquin-1 mutants (Figures 5C, S5C, and S5D), we showed that the A-site of the ROQ domain, which is required for RNA binding, as well as sequences located downstream of Arg510, the MALT1 cleavage site, were essential for the regulation of protein synthesis (Figures 5C and S5D), and neither of these mutants accumulated in P bodies or in arsenite-induced stress granules (Figures S5E and S5F).

We next investigated how Roquin regulates PI3K-mTOR signaling in Treg cells and $CD4^+$ T cells. Phosphorylation of the ribosomal protein S6 as readout of mTORC1 activity was more prominent in Treg cells from DKO^{Treg} mice compared to control Treg cells (Figure 5D). Furthermore, there was an increase in the PIP3-induced phosphorylation of the residue Thr308 as well as in the mTORC2-dependent phosphorylation of residue Ser473 of the Akt kinase (Figure 5E). We also analyzed the activation status of the mTOR pathway in $CD4^+$ T cells treated with 4′OH-tamoxifen to induce the deletion of Roquin-encoding alleles ($iDKO^T$), which recapitulated increased mTORC1-dependent phosphorylation of S6 and mTORC2-dependent phosphorylation of Akt Ser473 at the steady state (Figures 5F and S6A–S6C) but showed normal induction of the pathway after anti-CD3 and -CD28 stimulation (Figures S6A–S6C).

The transcription factor Foxo1 relocalized from the nucleus to the cytoplasm both when we induced deletion of Roquin-encoding alleles in *Rc3h1-2*$^{fl/fl}$; *Cd4-Cre-ERT2* $CD4^+$ T cells by 4′OH-tamoxifen treatment ($iDKO^T$) and in Treg cells from DKO^{Treg} mice (Figures 5G and 5H). The increased Akt activity in $CD4^+$ T cells and Treg cells could explain this re-localization, as the phosphorylation of Foxo1 by Akt is known to induce its translocation from the nucleus to the cytoplasm (Stone et al., 2015). In addition, decreased Foxo1 protein expression coincided with increased expression of the Foxo1-specific E3 ubiquitin ligase Itch when we inducibly deleted Roquin-encoding alleles in $iDKO^T$ $CD4^+$ T cells (Figure 5I). Consistently, sorted GFP^+ Treg cells from *Rc3h1-2*$^{fl/fl}$;*DEREG*;*CD4-Cre-ERT2* ($iDKO^T$DEREG) mice that had received tamoxifen gavage showed increased Itch levels (Figure S6D). Moreover, the level of Itch protein decreased upon Roquin-1 overexpression in MEF cells (Figure S6E), the Itch mRNA emerged as a direct target of Roquin in our PAR-CLIP dataset from these cells, and Roquin-1 downregulated an *ICOS* reporter gene linked to the 3′ half of the *Itch* 3′ UTR (Figures 5J and 5K). These data reveal the negative regulation of mTOR signaling and protein biosynthesis by Roquin and identify Itch, a negative regulator of Foxo1 (Xiao et al., 2014), as a downstream target of Roquin in the PI3K-Akt-Foxo1 pathway.

Roquin Interferes with Post-transcriptional Repression of Pten by miR-17∼92

As the Pten mRNA also emerged as a Roquin-bound target in the PAR-CLIP dataset, we asked whether Roquin affects PI3K signaling upstream of Foxo1. In fact, specific binding of *Itch*, *Pten*, and *Nfkbiz* mRNA was observed after immunoprecipitation and qPCR analysis by WT and the RING finger mutant of Roquin-1, while introduction of A-site mutations into the ROQ domain of Roquin abolished these interactions (Figures 6A and S6F). The mRNA and protein levels of Pten decreased when Roquin-encoding alleles were deleted by 4′OH-tamoxifen treatment in $iDKO^T$ T cells (Figures 6B and 6C), and inducible deletion of Roquin-encoding alleles in Treg cells decreased Pten and increased Itch protein levels (Figure 6D and S6G). Our PAR-CLIP data identified the interaction of Roquin with a predicted U-rich hepta-loop hairpin structure in the 3′ UTR of *Pten* (Figures 6E and 6F). This stem-loop structure overlaps with a miR-17 binding site, which is responsible for the miR-17∼92-mediated repression of *Pten* in T cells (Xiao et al., 2008). Strikingly, we found that miR-17 and miR-19a, two representative miRNAs of the miR-17∼92 cluster, were upregulated in DKO^T effector T cells (Figure 6G). This upregulation may also be attributed to some extent to the strong activation of these T cells, since the induction of miRNAs was still present but clearly reduced in naive DKO^T T cells (Figure 6G). Interestingly, the decrease of Pten protein observed in $iDKO^T$ $CD4^+$ T cells was

Figure 5. Roquin Inhibits PI3K-mTOR Signaling in Treg Cells and $CD4^+$ T Cells

(A) Cumulative distributions of fold-changes in translation efficiency (TE) for indicated mRNAs in mepazine- or DMSO pretreated and PMA/ionomycin-stimulated $CD4^+$ T cells.

(B and C) Flow cytometry analysis of metabolic labeling with L-homopropargylglycine (HPG) of untreated and tamoxifen-induced iDKO MEF cells (B) or *Rc3h1-2*$^{-/-}$ MEF cells expressing full-length WT or indicated mutants of Roquin-1 (C) displaying untransduced cells (dashed line), uninduced cells (−dox, black line), or cells treated with doxycycline for 14 hr (+dox, red line).

(D and E) Flow cytometry of phosphorylated ribosomal protein S6 (Ser235/236) (D) or phosphorylated Akt (Ser473 and Thr308) (E) from $CD4^+YFP^+$ T cells of WT and DKO^{Treg} mice.

(F and I) Immunoblot analyses of indicated proteins in $CD4^+$ T cell cultures from $iDKO^T$ mice left untreated (−tam) or treated with 4′ OH-tamoxifen (+tam).

(G and H) Flow cytometry imaging and quantification to determine Foxo1 and Draq5 colocalization in iDKO T cells generated as in (F).

(J) Reporter assay testing the regulation of overlapping fragments of the 3′ UTR of *Itch* (1–1,513 and 1,411–2,389) by flow cytometry in *Rc3h1-2*$^{-/-}$ untransduced MEF cells (dashed line) and transduced cells with (red line) or without (black line) doxycycline-inducible expression of Roquin-1.

(K) PAR-CLIP read coverage around the Roquin binding site in 3′ UTR of the *Itch* mRNA.

Data are representative of one experiment with three (D) or four (A, E) biological replicates per group, two independent experiments (B, C, I), four independent experiments (H), or three independent experiments (F, J, K). Statistical significance was calculated by unpaired (D, E, H [left]) or paired (H [right]), two-tailed Student's t test; *$p < 0.05$, **$p < 0.01$, and ***$p < 0.001$. Data are mean ± SEM.

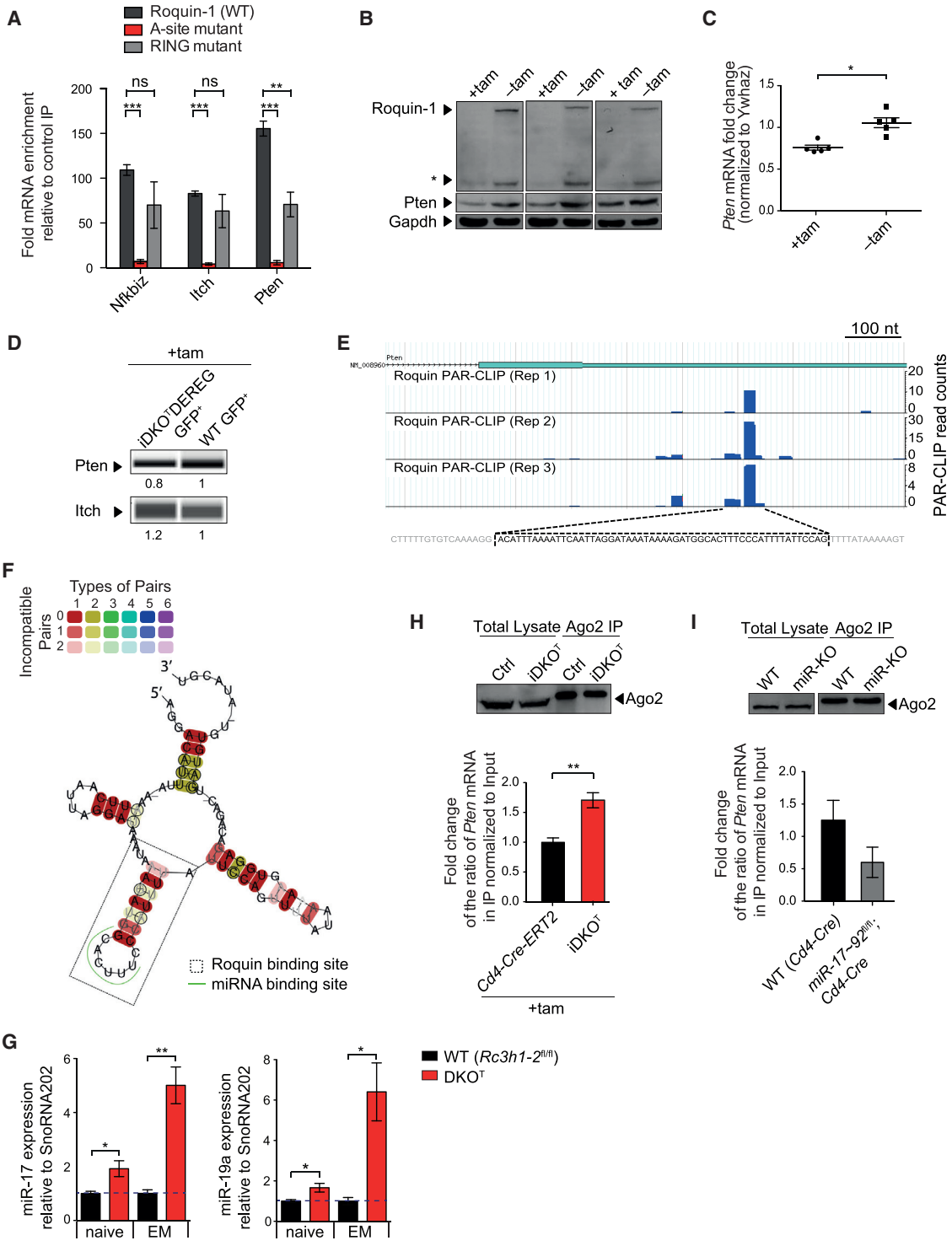

Figure 6. Roquin Promotes Pten Expression by Interfering with miR-17~92 Regulation

(A) Immunoprecipitation and RT-qPCR (RNA-IP) to detect the indicated mRNAs associated with Roquin-1 (WT) and Roquin-1 mutants (A-site [K220A K239A R260A] and RING [C14A]) normalized to the input and the corresponding ratio of the control IgG IP.

(B and D) Immunoblot analysis of indicated proteins in extracts from CD4$^+$ T cells from iDKO^T mice left untreated (–tam) or treated with 4′ OH-tamoxifen (+tam) (B) or sorted GFP$^+$ Treg cells from *DEREG; CD4-Cre-ERT2* (WT) mice or *Rc3h1-2$^{fl/fl}$; DEREG; CD4-Cre-ERT2* (iDKO^{T}DEREG) mice that received tamoxifen gavage (D).

(C and G) qPCR analysis of *Pten* (C) or miR-17, miR19a (G) gene expression in CD4$^+$ T cells from iDKO^T (C) or DKO^T mice (G).

(E) PAR-CLIP read coverage around the Roquin binding site in the 3′ UTR of *Pten* mRNA.

(legend continued on next page)

very comparable to the increase of the protein upon T cell-specific deletion of miR-17∼92 (Figure S6H). We then asked whether Roquin limits the access of the miRISC complex to the miR-17∼92 binding site in the 3′ UTR of *Pten*. Indeed, quantitative RT-PCR analysis of RNA associated with immunoprecipitated Ago2 demonstrated more association of Ago2 with the *Pten* mRNA in extracts from Roquin-deficient (iDKO^{T}) compared to control CD4^{+} T cells (Figure 6H). As expected, CD4^{+} T cells that lacked expression of miR-17∼92 showed decreased Ago2 protein interaction with the *Pten* mRNA (Figure 6I). Together, these data reveal an impact of Roquin on PI3K-mTOR signaling and provide a molecular basis for Roquin's influence on the cell fate not only of Treg but also of conventional T cells.

Roquin Shapes T Cell Differentiation by Inhibiting the PI3K-mTOR Pathway

We therefore addressed how deregulation of this pathway affects differentiation of Roquin-deficient CD4^{+} T cells by analyzing the reciprocal Th17 and iTreg cell differentiation programs (Figures 7A–7F and S7A–S7C). Despite increased numbers of thymus-derived Treg cells upon ablation of Roquin-encoding alleles *in vivo*, naive CD4^{+} T cells from these mice were strongly biased toward Th17 cell differentiation and impaired in iTreg cell differentiation *in vitro* (Figures 7A and 7B; Jeltsch et al., 2014). Nevertheless, the increased frequency of IL-17A-producing T cells or the reduced frequency of Foxp3-expressing iTreg cells in DKO^{T} cultures were readily corrected to frequencies of WT counterparts when DKO^{T} CD4^{+} T cells were differentiated in the presence of sub-optimal doses of rapamycin or LY294002 (Figures 7A and 7C), which did not affect IL-10 production in these cultures (Figure S7D). The use of the more selective PI3K p110δ-specific inhibitor PI-3065 (Ali et al., 2014) similarly rescued the differentiation of Roquin-deficient iTreg cells with much less impact on WT counterparts (Figure 7D and S7C). However, instead of inhibiting Th17 cell differentiation by reducing the number of IL-17-producing cells, this inhibitor rather reduced the expression level of IL-17A in DKO cells (Figure 7B) and even more strongly in WT T cells (Figures S7A and S7B). Comparing the effect of increasing doses of rapamycin on Th17 or iTreg cell differentiation of the different genotypes, DKO^{T} compared to WT T cells showed an enhanced or decreased responsiveness under iTreg or Th17 cell differentiation, respectively (Figures 7E and 7F). The lower sensitivity of Roquin-deficient T cells to rapamycin or PI-3065 under Th17 cell conditions may be explained by induced expression of additional Roquin target mRNAs, such as the Th17 cell-driving *Nfkbiz* and *Nfkbid* genes (Annemann et al., 2015; Jeltsch et al., 2014; Okamoto et al., 2010).

Finally, we tested the effect of mTOR inhibition on the induction of Tfh and GC B cells that is observed in iDKO^{T} mice 8 days after tamoxifen-induced deletion of Roquin-encoding alleles (Figures 7G–7I and S7E–S7I). Oral gavage with tamoxifen strongly decreased Roquin protein levels in extracts of iDKO^{T} CD4^{+} T cells pooled from mice of iDKO^{T} and iDKO^{T} mice treated with rapamycin or vehicle (Figure S7E). The administration of rapamycin to iDKO^{T} mice abolished the phosphorylation of S6K at Thr389 that was elevated in CD4^{+} T cells from iDKO^{T} mice (Figure S7E). Accumulation of GC Tfh and GC B cells after tamoxifen treatment was unchanged when mice were injected with vehicle only, but was significantly reduced when mice received rapamycin every second day (Figures 7H, 7I, and S7F–S7I). To exclude B cell-dependent effects of rapamycin, we treated μMT mice, which lack mature B cells, with vehicle or rapamycin as before (Figures 7J, 7K, S7J, and S7K). In the absence of B cells, the CD44^{hi} population of CD4^{+} T cells contained Tfh but not GC Tfh cells. Furthermore, induction of Tfh cells in μMT mice was strongly enhanced for adoptively transferred iDKO CD4^{+} T cells that were marked by YFP after tamoxifen-induced activation of Cre (Figure 7L). Importantly, rapamycin treatment effectively reduced B cell-independent differentiation of Tfh cells in endogenous (Figures 7J–7L and S7J–S7M) or adoptively transferred (Figures 7L, 7M, and S7L–S7M) Roquin-deficient T cells, indicating a B cell-independent requirement of PI3K-mTOR signaling during Tfh cell subset differentiation. These data support the conclusion that due to a pre-activated PI3K-mTOR pathway, Roquin-deficient CD4^{+} T cells inappropriately commit to Tfh or Th17 cell differentiation.

DISCUSSION

Roquin RNA-binding proteins are essential in limiting immune responses and preventing autoimmunity. Through their many targets, they probably modulate a variety of molecular pathways. In this study we have demonstrated that Roquin inhibits the PI3K-mTOR pathway, which regulates protein biogenesis and is important for T cell activation and fate decisions (Pollizzi and Powell, 2015). With inducible gene deletion we have uncovered a profound positive regulation of Pten by Roquin in conventional CD4^{+} and regulatory T cells. Pten is a crucial negative regulator of the PI3K-mTOR pathway, which is tightly controlled in T helper cells by miRNAs of the miR-17∼92 cluster (Baumjohann and Ansel, 2013). We found that Roquin not only reduced the levels of miR-17∼92 but also interfered with the interaction of these miRNAs with the *Pten* 3′ UTR by binding to an overlapping site that can pair in an ADE-type secondary structure (Janowski et al., 2016). We propose that Roquin binding to this stem-loop precludes base pairing of miR-17∼92 with the *Pten* 3′ UTR and thereby increases cellular Pten levels. A similar Pumilio-enforced RNA structure switch has been reported to limit access of miR-221 or miR-222 to their binding sites in the 3′ UTR of *p27*

(F) Predicted secondary structure of the mRNA sequence around the Roquin-binding site in the *Pten* 3′ UTR predicted. The base pairs are colored according to their conservation and the color saturation decreases with the number of incompatible base pairs found in different species.

(H and I) RNA-IP analysis with antibodies against Ago2 (Zhu et al., 2010) in extracts of 4′ OH-tamoxifen-treated CD4^{+} T cell cultures from WT and iDKO^{T} mice (H) or from WT and *miR-17∼92*$^{fl/fl}$; *Cd4-Cre* (miR-KO) mice (I). Immunoblots showing Ago2 protein in total lysate and after immunoprecipitation (top). The amount of *Pten* mRNA in the immunoprecipitates is displayed as percentage of input (bottom).

Data are representative of three independent experiments (A, B, E, I), five independent experiments (C, H), or two independent experiments (D) or in one experiment with three mice per group (G). Statistical significance was calculated by unpaired (A, G–I) or paired (C), two-tailed Student's t test; *$p < 0.05$ and **$p < 0.01$. Horizontal lines indicate mean and vertical error bars the standard error of the mean (±SEM).

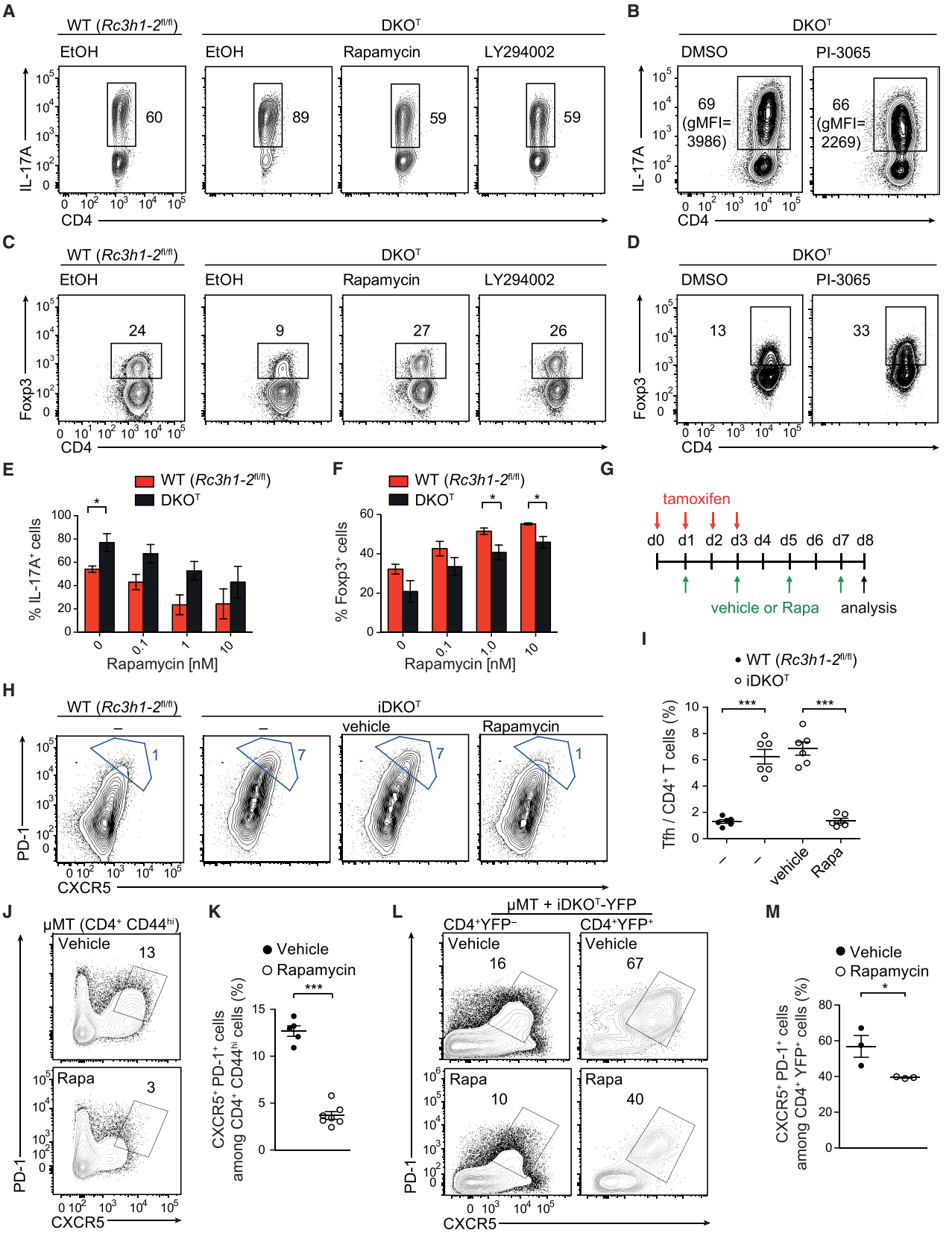

(legend on next page)

(Kedde et al., 2010). This type of regulation will depend on the relative expression levels of miR-17∼92 and Roquin and may enable cell-type- and context-specific control, since both factors are strongly regulated (Baumjohann and Ansel, 2013; Jeltsch and Heissmeyer, 2016). Consistent with this concept of dynamic regulation, analysis of Roquin-deficient NKT cells showed developmental skewing toward the NKT17 subset in the thymus associated with an absence of NKT cells in the periphery. Although this phenotype would be explained by derepressed mTORC1 activity as demonstrated by the strikingly similar phenotype of *Tsc1*$^{fl/fl}$*;CD4-Cre* mice (Wu et al., 2014), mature Roquin-deficient NKT17 cells in the thymus did not reveal increased mTOR phosphorylation (Drees et al., 2017).

A Roquin-mediated stimulation of the mTOR pathway has been reported before, the proposed molecular mechanism involving a Roquin RING-finger-dependent inhibition of the AMPK kinase that itself inhibits mTOR (Ramiscal et al., 2015). Our findings of Roquin-mediated negative regulation of mTOR signaling indicate either a parallel antagonistic function or an intra-molecular negative feedback regulation through the E3 ligase function of the RING finger in the Roquin protein.

How can our findings explain that Roquin-deficient T cells preferentially differentiate into Tfh and Th17 cell subsets and that Treg cells lacking Roquin are specialized to repress GC B cell responses but functionally impaired to repress T cell responses? There is a strong overlap of phenotypes that are caused in mice by T cell-specific deletion of Roquin-encoding alleles (Vogel et al., 2013) with those induced by transgenic overexpression of miR-17∼92 or heterozygous deletion of Pten in lymphocytes (Xiao et al., 2008). Also, deletion of Roquin- or Pten-encoding alleles in Treg cells elicits similar phenotypes (Huynh et al., 2015; Shrestha et al., 2015). Consistent with Foxo1 being a downstream target in this pathway, deletion of Foxo1 also effectively induces Tfh and Th17 cell differentiation, and expression of Foxo1 is required for Treg cell function (Kerdiles et al., 2010; Lainé et al., 2015; Stone et al., 2015). While our data did not support a general instability of Foxp3 expression *in vivo*, we have presented evidence for functional impairment of Roquin-deficient Treg cells: losing CD25 expression in a PI3K-dependent manner (Huynh et al., 2015), these Treg cells may consume less IL-2 and thereby may be less efficient in repressing the activation of CD8$^+$ T cells (Chinen et al., 2016). Despite the fact that these Treg cells express higher levels of IL-10 as well as of the Roquin-target CTLA-4, they appear less able to regulate *in vivo*. This lack of regulation could be related to the lack of Foxo-1-dependent CD62L (Kerdiles et al., 2009) and TGF-β-dependent CD103 expression (Kilshaw and Murant, 1991), the downregulation of Foxp3 target genes, as well as the strongly altered cytokine production by Treg cells, conventional T cells, and exTreg cells. To explain similarities and differences observed in Pten- and Roquin-deficient Treg cells, we propose a model in which Roquin deficiency and reduced Pten activity make Treg cells convert to Tfr cells, which remain effective to repress antigen-specific B cell responses while non-follicular Treg cell functions are impaired. Only upon strong or complete loss-of-function of Pten are both Tfr and non-follicular Treg cells rendered inactive as they lose Foxp3 expression and change cellular identity (Huynh et al., 2015; Shrestha et al., 2015).

PIP3K is effectively activated through the ICOS receptor, a well-established post-transcriptional target of Roquin (Glasmacher et al., 2010; Schlundt et al., 2014; Yu et al., 2007). PIP3 production then leads to the activation of the Akt kinase that phosphorylates Foxo1, a transcription factor that maintains T cells in a quiescent state (Kerdiles et al., 2010). This phosphorylation inactivates Foxo1 by re-localization to the cytoplasm and ubiquitination by the E3 ubiquitin ligase Itch (Xiao et al., 2014). The molecular program of PI3K and mTOR activation as well as Foxo1 inactivation following Roquin loss-of-function in T cells or Treg cells is therefore induced in three different ways: through increased ICOS signaling, through reduced *Pten* expression, and through more effective ubiquitination and degradation of Foxo1 due to increased levels of the Roquin target Itch. Given the general importance of the PI3K-mTOR signaling pathway and considering the ubiquitous expression of Roquin proteins, the newly uncovered regulation is expected to have a broad impact on metabolic programs and cell fate decisions in other immune and non-immune cells under homeostasis, when faced with environmental challenge, as well as during the development of cancer.

STAR★METHODS

Detailed methods are provided in the online version of this paper and include the following:

- KEY RESOURCES TABLE
- CONTACT FOR REAGENT AND RESOURCE SHARING
- EXPERIMENTAL MODEL AND SUBJECT DETAILS
  - Mice
- METHOD DETAILS
  - Immunization with NP-KLH
  - ELISA
  - *In vivo* colitis model
  - Histology
  - Cell Culture of MEF and T cells

Figure 7. Roquin Shapes T Cell Differentiation by Inhibiting the PI3K-mTOR Pathway

(A–F) Th17 (A, B, E) or Treg (C, D, F) cell cultures from naive CD4$^+$ T cells isolated from WT and DKO^T mice and supplemented with the indicated inhibitors were analyzed by flow cytometry (A–D) and quantified (E–F).

(G–I) Mice were gavaged with tamoxifen and injected with either rapamycin or vehicle or left untreated as depicted (G). Flow cytometric analysis (H) and frequencies (I) of Tfh cells.

(J–M) μMT mice were treated only with vehicle or rapamycin as in (G) or received adoptive transfer of CD4$^+$ T cells from iDKO mice marked with YFP to track Cre activity before treatment with tamoxifen and rapamycin as well as induction of Tfh cells with SRBCs as shown in Figure S7K. Tfh cell markers were analyzed on CD4$^+$ T cells pregated for CD44^{hi} T cells (J, K) or YFP$^-$ and YFP$^+$ (L).

Data are representative of three independent experiments (A, B, E), four independent experiments (C, F), two independent experiments (D), or one experiment with six or three mice per group (H–M). Statistical significance was calculated by two-tailed Student's t test; *$p < 0.05$ and ***$p < 0.001$. Horizontal lines indicate mean and vertical error bars the standard error of the mean (±SEM).

SUPPLEMENTAL INFORMATION

Supplemental Information includes seven figures and can be found with this article online at https://doi.org/10.1016/j.immuni.2017.11.008.

AUTHOR CONTRIBUTIONS

K.E., D.H., S.E., and V.H. conceived the project and designed the experiments with input from D.A., J.C.G., M.Z., A.B.K., C.F.C., J.H., H.L., and D.B. Most experiments were performed by K.E. and D.H. Bioinformatics analyses were performed by J.C.G. D.A., T.R., J. Kranich, G.B., S.E., A.H., J. Klein, A.M., S.F., and E.N. contributed individual experiments. S.M. and M.H.A enabled the use of unpublished reagents. The manuscript was written by K.E., D.H., and V.H. with critical input from D.B., J.C.G., A.B.K., T.B., J.H., E.N., and M.Z.

ACKNOWLEDGMENTS

We thank Frank Dahlström, Claudia Lohs, Desiree Argiriu, and Barbara Mosetter for technical assistance and Kai Höfig for advice. For the provision of mice, we thank Thorsten Buch (*Cd4-Cre-ERT2*), Marc Schmidt-Supprian (*Rc3h1*^{fl}), Wolfgang Wurst (*Rc3h2*^{fl}), Alexander Y. Rudensky (*Foxp3-IRES-YFP-Cre*), Tim Sparwasser (DEREG), and Christopher Wilson (*Cd4-Cre*). J.C.G. was supported by a SystemsX.ch Transitional Postdoctoral Fellowship and D.B. by the Emmy Noether Programme of the DFG (BA 5132/1-1). The work was supported by the DFG grants HE3359/4-1 to V.H. and KR2199/3-2 and KR2199/9-1 to A.B.K., SFB 1243 project A01 to H.L., SFB 854 project B16 to J.H., SPP-1935 to V.H., the SFB-1054 projects A03 and Z02 to V.H., A06 to A.B.K., B03 to T.B., B12 to D.B., as well as by Friedrich-Baur foundation grants to D.H. and A.H., and an Erich and Gertrud Roggenbuck Foundation grant (218-15) to E.N. as well as by an European Research Council ERC-StG (no. 281666 Rc3h1/2-Specificity), a Fritz Thyssen foundation (10.16.1.021MN), and an ElseFresenius-Kröner foundation grant (2015_A158) to V.H.

Received: January 5, 2017
Revised: July 20, 2017
Accepted: November 6, 2017
Published: December 12, 2017

REFERENCES

Ali, K., Soond, D.R., Pineiro, R., Hagemann, T., Pearce, W., Lim, E.L., Bouabe, H., Scudamore, C.L., Hancox, T., Maecker, H., et al. (2014). Inactivation of PI(3)K p110δ breaks regulatory T-cell-mediated immune tolerance to cancer. Nature *510*, 407–411.

Annemann, M., Wang, Z., Plaza-Sirvent, C., Glauben, R., Schuster, M., Ewald Sander, F., Mamareli, P., Kühl, A.A., Siegmund, B., Lochner, M., and Schmitz, I. (2015). IκBNS regulates murine Th17 differentiation during gut inflammation and infection. J. Immunol. *194*, 2888–2898.

Balwierz, P.J., Pachkov, M., Arnold, P., Gruber, A.J., Zavolan, M., and van Nimwegen, E. (2014). ISMARA: automated modeling of genomic signals as a democracy of regulatory motifs. Genome Res. *24*, 869–884.

Baumjohann, D., and Ansel, K.M. (2013). MicroRNA-mediated regulation of T helper cell differentiation and plasticity. Nat. Rev. Immunol. *13*, 666–678.

Baumjohann, D., Kageyama, R., Clingan, J.M., Morar, M.M., Patel, S., de Kouchkovsky, D., Bannard, O., Bluestone, J.A., Matloubian, M., Ansel, K.M., and Jeker, L.T. (2013a). The microRNA cluster miR-17∼92 promotes TFH cell differentiation and represses subset-inappropriate gene expression. Nat. Immunol. *14*, 840–848.

Baumjohann, D., Preite, S., Reboldi, A., Ronchi, F., Ansel, K.M., Lanzavecchia, A., and Sallusto, F. (2013b). Persistent antigen and germinal center B cells sustain T follicular helper cell responses and phenotype. Immunity *38*, 596–605.

Bertossi, A., Aichinger, M., Sansonetti, P., Lech, M., Neff, F., Pal, M., Wunderlich, F.T., Anders, H.J., Klein, L., and Schmidt-Supprian, M. (2011). Loss of Roquin induces early death and immune deregulation but not autoimmunity. J. Exp. Med. *208*, 1749–1756.

Chinen, T., Kannan, A.K., Levine, A.G., Fan, X., Klein, U., Zheng, Y., Gasteiger, G., Feng, Y., Fontenot, J.D., and Rudensky, A.Y. (2016). An essential role for the IL-2 receptor in Treg cell function. Nat. Immunol. *17*, 1322–1333.

Chung, Y., Tanaka, S., Chu, F., Nurieva, R.I., Martinez, G.J., Rawal, S., Wang, Y.H., Lim, H., Reynolds, J.M., Zhou, X.H., et al. (2011). Follicular regulatory T cells expressing Foxp3 and Bcl-6 suppress germinal center reactions. Nat. Med. *17*, 983–988.

Delgoffe, G.M., Kole, T.P., Zheng, Y., Zarek, P.E., Matthews, K.L., Xiao, B., Worley, P.F., Kozma, S.C., and Powell, J.D. (2009). The mTOR kinase differentially regulates effector and regulatory T cell lineage commitment. Immunity *30*, 832–844.

Delgoffe, G.M., Pollizzi, K.N., Waickman, A.T., Heikamp, E., Meyers, D.J., Horton, M.R., Xiao, B., Worley, P.F., and Powell, J.D. (2011). The kinase mTOR regulates the differentiation of helper T cells through the selective activation of signaling by mTORC1 and mTORC2. Nat. Immunol. *12*, 295–303.

Drees, C., Vahl, J.C., Bortoluzzi, S., Heger, K.D., Fischer, J.C., Wunderlich, F.T., Peschel, C., and Schmidt-Supprian, M. (2017). Roquin paralogs differentially regulate functional NKT cell subsets. J. Immunol. *198*, 2747–2759.

Floess, S., Freyer, J., Siewert, C., Baron, U., Olek, S., Polansky, J., Schlawe, K., Chang, H.D., Bopp, T., Schmitt, E., et al. (2007). Epigenetic control of the foxp3 locus in regulatory T cells. PLoS Biol. *5*, e38.

Gerriets, V.A., Kishton, R.J., Johnson, M.O., Cohen, S., Siska, P.J., Nichols, A.G., Warmoes, M.O., de Cubas, A.A., MacIver, N.J., Locasale, J.W., et al. (2016). Foxp3 and Toll-like receptor signaling balance Treg cell anabolic metabolism for suppression. Nat. Immunol. *17*, 1459–1466.

Gewies, A., Gorka, O., Bergmann, H., Pechloff, K., Petermann, F., Jeltsch, K.M., Rudelius, M., Kriegsmann, M., Weichert, W., Horsch, M., et al. (2014). Uncoupling Malt1 threshold function from paracaspase activity results in destructive autoimmune inflammation. Cell Rep. *9*, 1292–1305.

Glasmacher, E., Hoefig, K.P., Vogel, K.U., Rath, N., Du, L., Wolf, C., Kremmer, E., Wang, X., and Heissmeyer, V. (2010). Roquin binds inducible costimulator mRNA and effectors of mRNA decay to induce microRNA-independent post-transcriptional repression. Nat. Immunol. *11*, 725–733.

Hafner, M., Landthaler, M., Burger, L., Khorshid, M., Hausser, J., Berninger, P., Rothballer, A., Ascano, M., Jr., Jungkamp, A.C., Munschauer, M., et al. (2010). Transcriptome-wide identification of RNA-binding protein and microRNA target sites by PAR-CLIP. Cell *141*, 129–141.

Hafner, M., Renwick, N., Farazi, T.A., Mihailović, A., Pena, J.T., and Tuschl, T. (2012). Barcoded cDNA library preparation for small RNA profiling by next-generation sequencing. Methods *58*, 164–170.

Haxhinasto, S., Mathis, D., and Benoist, C. (2008). The AKT-mTOR axis regulates de novo differentiation of CD4+Foxp3+ cells. J. Exp. Med. *205*, 565–574.

Hoffmann, S., Otto, C., Kurtz, S., Sharma, C.M., Khaitovich, P., Vogel, J., Stadler, P.F., and Hackermüller, J. (2009). Fast mapping of short sequences with mismatches, insertions and deletions using index structures. PLoS Comput. Biol. *5*, e1000502.

Hsieh, A.C., Liu, Y., Edlind, M.P., Ingolia, N.T., Janes, M.R., Sher, A., Shi, E.Y., Stumpf, C.R., Christensen, C., Bonham, M.J., et al. (2012). The translational landscape of mTOR signalling steers cancer initiation and metastasis. Nature *485*, 55–61.

Huynh, A., DuPage, M., Priyadharshini, B., Sage, P.T., Quiros, J., Borges, C.M., Townamchai, N., Gerriets, V.A., Rathmell, J.C., Sharpe, A.H., et al. (2015). Control of PI(3) kinase in Treg cells maintains homeostasis and lineage stability. Nat. Immunol. *16*, 188–196.

Janowski, R., Heinz, G.A., Schlundt, A., Wommelsdorf, N., Brenner, S., Gruber, A.R., Blank, M., Buch, T., Buhmann, R., Zavolan, M., et al. (2016). Roquin recognizes a non-canonical hexaloop structure in the 3′-UTR of Ox40. Nat. Commun. *7*, 11032.

Jeltsch, K.M., and Heissmeyer, V. (2016). Regulation of T cell signaling and autoimmunity by RNA-binding proteins. Curr. Opin. Immunol. *39*, 127–135.

Jeltsch, K.M., Hu, D., Brenner, S., Zöller, J., Heinz, G.A., Nagel, D., Vogel, K.U., Rehage, N., Warth, S.C., Edelmann, S.L., et al. (2014). Cleavage of roquin and regnase-1 by the paracaspase MALT1 releases their cooperatively repressed targets to promote T(H)17 differentiation. Nat. Immunol. *15*, 1079–1089.

Kang, S.G., Liu, W.H., Lu, P., Jin, H.Y., Lim, H.W., Shepherd, J., Fremgen, D., Verdin, E., Oldstone, M.B., Qi, H., et al. (2013). MicroRNAs of the miR-17∼92 family are critical regulators of T(FH) differentiation. Nat. Immunol. *14*, 849–857.

Kedde, M., van Kouwenhove, M., Zwart, W., Oude Vrielink, J.A., Elkon, R., and Agami, R. (2010). A Pumilio-induced RNA structure switch in p27-3′ UTR controls miR-221 and miR-222 accessibility. Nat. Cell Biol. *12*, 1014–1020.

Kerdiles, Y.M., Beisner, D.R., Tinoco, R., Dejean, A.S., Castrillon, D.H., DePinho, R.A., and Hedrick, S.M. (2009). Foxo1 links homing and survival of naive T cells by regulating L-selectin, CCR7 and interleukin 7 receptor. Nat. Immunol. *10*, 176–184.

Kerdiles, Y.M., Stone, E.L., Beisner, D.R., McGargill, M.A., Ch'en, I.L., Stockmann, C., Katayama, C.D., and Hedrick, S.M. (2010). Foxo transcription factors control regulatory T cell development and function. Immunity *33*, 890–904.

Khorshid, M., Rodak, C., and Zavolan, M. (2011). CLIPZ: a database and analysis environment for experimentally determined binding sites of RNA-binding proteins. Nucleic Acids Res. *39*, D245–D252.

Kilshaw, P.J., and Murant, S.J. (1991). Expression and regulation of beta 7(beta p) integrins on mouse lymphocytes: relevance to the mucosal immune system. Eur. J. Immunol. *21*, 2591–2597.

Kurebayashi, Y., Nagai, S., Ikejiri, A., Ohtani, M., Ichiyama, K., Baba, Y., Yamada, T., Egami, S., Hoshii, T., Hirao, A., et al. (2012). PI3K-Akt-mTORC1-S6K1/2 axis controls Th17 differentiation by regulating Gfi1 expression and nuclear translocation of RORγ. Cell Rep. *1*, 360–373.

Lahl, K., and Sparwasser, T. (2011). In vivo depletion of FoxP3+ Tregs using the DEREG mouse model. Methods Mol. Biol. *707*, 157–172.

Lainé, A., Martin, B., Luka, M., Mir, L., Auffray, C., Lucas, B., Bismuth, G., and Charvet, C. (2015). Foxo1 is a T cell-intrinsic inhibitor of the RORγt-Th17 program. J. Immunol. *195*, 1791–1803.

Lee, K., Gudapati, P., Dragovic, S., Spencer, C., Joyce, S., Killeen, N., Magnuson, M.A., and Boothby, M. (2010). Mammalian target of rapamycin protein complex 2 regulates differentiation of Th1 and Th2 cell subsets via distinct signaling pathways. Immunity *32*, 743–753.

Leppek, K., Schott, J., Reitter, S., Poetz, F., Hammond, M.C., and Stoecklin, G. (2013). Roquin promotes constitutive mRNA decay via a conserved class of stem-loop recognition motifs. Cell *153*, 869–881.

Linterman, M.A., Pierson, W., Lee, S.K., Kallies, A., Kawamoto, S., Rayner, T.F., Srivastava, M., Divekar, D.P., Beaton, L., Hogan, J.J., et al. (2011). Foxp3+ follicular regulatory T cells control the germinal center response. Nat. Med. *17*, 975–982.

Love, M.I., Huber, W., and Anders, S. (2014). Moderated estimation of fold change and dispersion for RNA-seq data with DESeq2. Genome Biol. *15*, 550.

Okamoto, K., Iwai, Y., Oh-Hora, M., Yamamoto, M., Morio, T., Aoki, K., Ohya, K., Jetten, A.M., Akira, S., Muta, T., and Takayanagi, H. (2010). IkappaBzeta regulates T(H)17 development by cooperating with ROR nuclear receptors. Nature *464*, 1381–1385.

Olshen, A.B., Hsieh, A.C., Stumpf, C.R., Olshen, R.A., Ruggero, D., and Taylor, B.S. (2013). Assessing gene-level translational control from ribosome profiling. Bioinformatics *29*, 2995–3002.

Pollizzi, K.N., and Powell, J.D. (2015). Regulation of T cells by mTOR: the known knowns and the known unknowns. Trends Immunol. *36*, 13–20.

Ramiscal, R.R., Parish, I.A., Lee-Young, R.S., Babon, J.J., Blagih, J., Pratama, A., Martin, J., Hawley, N., Cappello, J.Y., Nieto, P.F., et al. (2015). Attenuation of AMPK signaling by ROQUIN promotes T follicular helper cell formation. eLife *4*, 4.

Rolf, J., Bell, S.E., Kovesdi, D., Janas, M.L., Soond, D.R., Webb, L.M., Santinelli, S., Saunders, T., Hebeis, B., Killeen, N., et al. (2010). Phosphoinositide 3-kinase activity in T cells regulates the magnitude of the germinal center reaction. J. Immunol. *185*, 4042–4052.

Rubtsov, Y.P., Rasmussen, J.P., Chi, E.Y., Fontenot, J., Castelli, L., Ye, X., Treuting, P., Siewe, L., Roers, A., Henderson, W.R., Jr., et al. (2008). Regulatory T cell-derived interleukin-10 limits inflammation at environmental interfaces. Immunity *28*, 546–558.

Sauer, S., Bruno, L., Hertweck, A., Finlay, D., Leleu, M., Spivakov, M., Knight, Z.A., Cobb, B.S., Cantrell, D., O'Connor, E., et al. (2008). T cell receptor signaling controls Foxp3 expression via PI3K, Akt, and mTOR. Proc. Natl. Acad. Sci. USA *105*, 7797–7802.

Schlundt, A., Heinz, G.A., Janowski, R., Geerlof, A., Stehle, R., Heissmeyer, V., Niessing, D., and Sattler, M. (2014). Structural basis for RNA recognition in roquin-mediated post-transcriptional gene regulation. Nat. Struct. Mol. Biol. *21*, 671–678.

Shrestha, S., Yang, K., Guy, C., Vogel, P., Neale, G., and Chi, H. (2015). Treg cells require the phosphatase PTEN to restrain TH1 and TFH cell responses. Nat. Immunol. *16*, 178–187.

Stone, E.L., Pepper, M., Katayama, C.D., Kerdiles, Y.M., Lai, C.Y., Emslie, E., Lin, Y.C., Yang, E., Goldrath, A.W., Li, M.O., et al. (2015). ICOS coreceptor signaling inactivates the transcription factor FOXO1 to promote Tfh cell differentiation. Immunity *42*, 239–251.

Thoreen, C.C., Chantranupong, L., Keys, H.R., Wang, T., Gray, N.S., and Sabatini, D.M. (2012). A unifying model for mTORC1-mediated regulation of mRNA translation. Nature *485*, 109–113.

Vinuesa, C.G., Cook, M.C., Angelucci, C., Athanasopoulos, V., Rui, L., Hill, K.M., Yu, D., Domaschenz, H., Whittle, B., Lambe, T., et al. (2005). A RING-type ubiquitin ligase family member required to repress follicular helper T cells and autoimmunity. Nature *435*, 452–458.

Vogel, K.U., Edelmann, S.L., Jeltsch, K.M., Bertossi, A., Heger, K., Heinz, G.A., Zöller, J., Warth, S.C., Hoefig, K.P., Lohs, C., et al. (2013). Roquin paralogs

1 and 2 redundantly repress the Icos and Ox40 costimulator mRNAs and control follicular helper T cell differentiation. Immunity *38*, 655–668.

Wollenberg, I., Agua-Doce, A., Hernández, A., Almeida, C., Oliveira, V.G., Faro, J., and Graca, L. (2011). Regulation of the germinal center reaction by Foxp3+ follicular regulatory T cells. J. Immunol. *187*, 4553–4560.

Wu, J., Yang, J., Yang, K., Wang, H., Gorentla, B., Shin, J., Qiu, Y., Que, L.G., Foster, W.M., Xia, Z., et al. (2014). iNKT cells require TSC1 for terminal maturation and effector lineage fate decisions. J. Clin. Invest. *124*, 1685–1698.

Xiao, C., Srinivasan, L., Calado, D.P., Patterson, H.C., Zhang, B., Wang, J., Henderson, J.M., Kutok, J.L., and Rajewsky, K. (2008). Lymphoproliferative disease and autoimmunity in mice with increased miR-17-92 expression in lymphocytes. Nat. Immunol. *9*, 405–414.

Xiao, N., Eto, D., Elly, C., Peng, G., Crotty, S., and Liu, Y.C. (2014). The E3 ubiquitin ligase Itch is required for the differentiation of follicular helper T cells. Nat. Immunol. *15*, 657–666.

Yang, B.H., Hagemann, S., Mamareli, P., Lauer, U., Hoffmann, U., Beckstette, M., Föhse, L., Prinz, I., Pezoldt, J., Suerbaum, S., et al. (2016a). Foxp3(+) T cells expressing RORγt represent a stable regulatory T-cell effector lineage with enhanced suppressive capacity during intestinal inflammation. Mucosal Immunol. *9*, 444–457.

Yang, J., Lin, X., Pan, Y., Wang, J., Chen, P., Huang, H., Xue, H.H., Gao, J., and Zhong, X.P. (2016b). Critical roles of mTOR Complex 1 and 2 for T follicular helper cell differentiation and germinal center responses. eLife *5*, 5.

Yu, D., Tan, A.H., Hu, X., Athanasopoulos, V., Simpson, N., Silva, D.G., Hutloff, A., Giles, K.M., Leedman, P.J., Lam, K.P., et al. (2007). Roquin represses autoimmunity by limiting inducible T-cell co-stimulator messenger RNA. Nature *450*, 299–303.

Zeng, H., Cohen, S., Guy, C., Shrestha, S., Neale, G., Brown, S.A., Cloer, C., Kishton, R.J., Gao, X., Youngblood, B., et al. (2016). mTORC1 and mTORC2 kinase signaling and glucose metabolism drive follicular helper T cell differentiation. Immunity *45*, 540–554.

Zhu, J.Y., Strehle, M., Frohn, A., Kremmer, E., Höfig, K.P., Meister, G., and Adler, H. (2010). Identification and analysis of expression of novel microRNAs of murine gammaherpesvirus 68. J. Virol. *84*, 10266–10275.

STAR★METHODS

KEY RESOURCES TABLE

REAGENT or RESOURCE	SOURCE	IDENTIFIER
Antibodies		
Ago2 (6F4)	Zhu et al., 2010	N/A
Roquin-1 and Roquin-2 (3F12 and 18F8)	Vogel et al., 2013; Jeltsch et al., 2014	N/A
Roquin-1	Bethyl Laboratories	Cat# A300-515A; RRID: AB_2179732
Phospho-mTOR (Ser2488) (D9C2)	Cell Signaling Technologies	Cat# 2971; RRID: AB_330970
mTOR (7C10)	Cell Signaling Technologies	Cat# 2983; RRID: AB_2105622
Phospho-p70 S6K (T389) (108D2)	Cell Signaling Technologies	Cat# 9234; RRID: AB_2269803
p70 S6K (49D7)	Cell Signaling Technologies	Cat# 2708; RRID: AB_390722
p70 S6Kα (H-9)	Santa Cruz Biotech	Cat# sc-8418; RRID: AB_628094
Phospho-S6 (S235/236) (D57.2.2E)	Cell Signaling Technologies	Cat# 4858; RRID: AB_916156
S6 (5G10)	Cell Signaling Technologies	Cat# 2217; RRID: AB_331355
Phospho-Akt (S473) (D9E)	Cell Signaling Technologies	Cat# 4060; RRID: AB_2315049; Cat# 4075 (AF647); RRID: AB_10691856
Phospho-Akt (T308) (D25E6)	Cell Signaling Technologies	Cat# 13038; RRID: AB_2629447; Cat# 13842 (PE)
Akt	Cell Signaling Technologies	Cat #9272; RRID: AB_329827
Phospho-Tsc2 (S939)	Cell Signaling Technologies	Cat# 3615; RRID: AB_2207796
Tsc2 (D93F12)	Cell Signaling Technologies	Cat# 4308; RRID: AB_10547134
Tsc1 (D43E2)	Cell Signaling Technologies	Cat# 6935; RRID: AB_10860420
Pten (D4.3)	Cell Signaling Technologies	Cat# 9188; RRID: AB_2253290
Pten (A2B1)	BD Biosciences	Cat# 559600; RRID: AB_397290
FoxO1 (C29H4)	Cell Signaling Technologies	Cat# 2880; RRID: AB_2106495
Anti-rabbit IgG, HRP-linked	Cell Signaling Technologies	Cat# 7074; RRID: AB_2099233
Anti-mouse IgG, HRP-linked	Cell Signaling Technologies	Cat# 7076; RRID: AB_330924
Anti-rat IgG, HRP-linked	Cell Signaling Technologies	Cat# 7077; RRID: AB_10694715
Itch (32/Itch)	BD Biosciences	Cat# 611198; RRID: AB_398732
CD25 (PC61)	BD Biosciences	Cat# 553866 (PE); RRID: AB_395101
IL-10 (JES5-16E3)	BD Biosciences	Cat# 554468 (APC); RRID: AB_398558
Bcl6 (K112-91)	BD Biosciences	Cat# 563363 (BV421)
CD95 (JO2)	BD Biosciences	Cat# 557653 (PE-Cy7); RRID: AB_396768
Goat anti-rabbit IgG	BD Biosciences	Cat# 554020 (FITC); RRID: AB_395212
GL7	BD Biosciences	Cat# 562080 (FITC); RRID: AB_10894953
GL7	BioLegend	Cat# 144605 (AF647); RRID: AB_2562184
CXCR5 (L138D7)	BioLegend	Cat# 145506 (APC); RRID: AB_2561970
IL-4 (11B11)	BioLegend	Cat# 504115; RRID: AB_2295885
CD304 Neuropilin-1 (3E12)	BioLegend	Cat# 145213 (biotin); RRID: AB_2687310
Tubulin (B-5-1-2)	Santa Cruz Biotech	Cat# sc-23948; RRID: AB_628410
G3BP1 (TT-Y)	Santa Cruz Biotech	Cat# sc-81940; RRID: AB_1123055
Normal rabbit IgG	Santa Cruz Biotech	Cat# sc-2027; RRID: AB_737197
Glut1 (EPR3915)	Abcam	Cat# ab115730; RRID: AB_10903230
GAPDH (6C5)	Calbiochem	Cat# CB1001; RRID: AB_2107426
IκBζ (LK2NAP)	eBioscience	Cat# 14-6801-82; RRID: AB_11218083
CD90.1 (Thy-1.1) (HIS51)	eBioscience	Cat# 17-0900-82 (APC); RRID: AB_469420
CD278 (hICOS) (ISA-3)	eBioscience	Cat# 13-9948-82 (biotin); RRID: AB_467004

(*Continued on next page*)

Continued

REAGENT or RESOURCE	SOURCE	IDENTIFIER
CD4 (GK1.5)	eBioscience	Cat# 48-0041-82 (eF450); RRID: AB_10718983; Cat# 11-0041-82 (FITC); RRID: AB_464892; Cat# 17-0041-82 (APC); RRID: AB_469320
CD4 (RM4-5)	BioLegend	Cat# 100531 (BV510); RRID: AB_2561388
CD8a (53-6.7)	eBioscience	Cat# 48-0081-82 (eF450); RRID: AB_1272198
B220 (RA3-6B2)	eBioscience	Cat# 45-0452-82 (PerCP-Cy5.5); RRID: AB_1107006; Cat# 13-0452-82 (biotin); RRID: AB_466449
CD62L (MEL-14)	eBioscience	Cat# 12-0621-82 (PE); RRID: AB_465721
PD-1 (J43)	eBioscience	Cat# 12-9985-82 (PE); RRID: AB_466295
CD122 (5H4)	eBioscience	Cat# 12-1221-82 (PE); RRID: AB_465833
GITR (DTA-1)	eBioscience	Cat# 46-5875-42 (PerCP-eF710); RRID: AB_2573783
CD134 OX40 (OX-86)	eBioscience	Cat# 17-1341-82 (APC); RRID: AB_10717260
CD103 (2E7)	eBioscience	Cat# 12-1031-82 (PE); RRID: AB_465799
ICOS (7E.17G9)	eBioscience	Cat# 25-9942-82 (PE-Cy7); RRID: AB_2573564
CD45.1 (A20)	eBioscience	Cat# 12-0453-82 (PE); RRID: AB_465675
CD45.2 (104)	eBioscience	Cat# 17-0454-82 (APC); RRID: AB_469400
Foxp3 (FJK-16 s)	eBioscience	Cat# 11-5773-82 (FITC); RRID: AB_465243; Cat# 13-5773-82 (biotin); RRID: AB_763540
HELIOS (22F6)	eBioscience	Cat# 46-9883-42 (PerCp-eF710); RRID: AB_2573924
Ki-67 (SolA15)	eBioscience	Cat# 12-5698-80 (PE); RRID: AB_11149672
CTLA4 (UC10-4B9)	eBioscience	Cat# 17-1522-82 (APC); RRID: AB_2016700
IL-17A (eBio17B7)	eBioscience	Cat# 48-7177-82 (eF450); RRID: AB_11149503
IL-17A (TC11-18H10.1)	BioLegend	Cat# 506904 (PE); RRID: AB_315464
IFN-γ (XMG1.2)	eBioscience	Cat# 45-7311-82 (PerCP-Cy5.5); RRID: AB_1107020
IFN-γ (XMG1.2)	BioLegend	Cat# 505827; RRID: AB_2295769
IL-2 (JES6-5H4)	eBioscience	Cat# 12-7021-82 (PE); RRID: AB_466150
CCR7 (4B12)	eBioscience	Cat# 17-1971-82 (APC); RRID: AB_469444
c-Maf (sym0F1)	eBioscience	Cat# 46-9855-42 (PerCP-eF710); RRID: AB_2573908
CD44 (IM7)	eBioscience	Cat# 17-0441-82 (APC); RRID: AB_469390
CD44 (IM7)	Tonbo Biosciences	Cat# 60-0441 (PE-Cy7); RRID: AB_2621847
CD3 (145-2C11)	Tonbo Biosciences	Cat# 70-0031; RRID: AB_2621472
CD3e (145-2C11)	BD Biosciences	Cat# 553064 (PE); RRID: AB_394597; Cat# 561826 (APC); RRID: AB_10896663
CD3 (145-2C11)	Helmholtz Zentrum München	in house
CD28 (37.51)	Tonbo Biosciences	Cat# 70-0281; RRID: AB_2621492
CD28 (37N)	Helmholtz Zentrum München	in house
CD16/32 (2.4G2)	Helmholtz Zentrum München	in house
Goat anti-mouse IgG; human-ads UNLB	Southern Biotech	Cat# 1030-01; RRID: AB_609693
Goat anti-mouse IgG1; human-ads UNLB	Southern Biotech	Cat# 1070-01
Goat anti-mouse IgGM; human-ads UNLB	Southern Biotech	Cat# 1020-01; RRID: AB_618651
Goat anti-mouse IgG-AP	Southern Biotech	Cat# 1030-04; RRID: AB_609689
Goat anti-mouse IgG1-AP	Southern Biotech	Cat# 1071-04
Goat anti-mouse IgM, human ads-BIOT	Southern Biotech	Cat# 1020-08; RRID: AB_616726

(*Continued on next page*)

Continued

REAGENT or RESOURCE	SOURCE	IDENTIFIER
Mouse IgG-UNLB	Southern Biotech	Cat# 0107-01
Mouse IgG1-UNLB	Southern Biotech	Cat# 0102-01
Mouse IgM-UNLB	Southern Biotech	Cat# 0101-01; RRID: AB_2629437
Goat anti-hamster IgG	MP Biochemicals	Cat# 0855397; RRID: AB_2334453
Goat anti-rabbit IgG	Invitrogen	Cat# A-11037 (AF594); RRID: AB_2534095; Cat# A-21244 (AF647); RRID: AB_2534074
Goat anti-rat IgG	Invitrogen	Cat# A-11006 (AF 488); RRID: AB_2534074
Goat anti-mouse IgG	Biotium	Cat# #20080 (CF405S); RRID: AB_10559051
Chemicals, Peptides, and Recombinant Proteins		
Cell Proliferation Dye eF450	eBioscience	Cat# 65-0842-85
Fixable Viability Dye eFluor 780	eBioscience	Cat# 65-0865-14
eBioscience Foxp3 / Transcription Factor Staining buffer set	Invitrogen	Cat# 00-5523-00
eBioscience IC Fixation Buffer	Invitrogen	Cat# 00-8222-49
SUPERase●In RNase Inhibitor	Invitrogen	Cat# AM2694
Acid phenol:chloroform:isoamyl alcohol (125:24:1, pH 4.5)	Invitrogen	Cat# AM9720
Dynabeads Protein G	Invitrogen	Cat# 10004D
Streptavidin, Alexa Fluor 555 Conjugate	Invitrogen	Cat# S32355
Cytofix Fixation Buffer	BD Biosciences	Cat# 554655
Phosflow Perm Buffer III	BD Biosciences	Cat# 558050
DRAQ5	Abcam	Cat# ab108410
Doxycycline hyclate	Sigma-Aldrich	Cat# D9891
LY-294002	Sigma-Aldrich	Cat# L9908
DMSO	Sigma-Aldrich	Cat# 276855
Cycloheximide	Sigma-Aldrich	Cat# C4859
Brefeldin A	Sigma-Aldrich	Cat# B7651
(Z)-4' OH-tamoxifen	Sigma-Aldrich	Cat# H7904
Tamoxifen	Sigma-Aldrich	Cat# T5648
SigmaFast p-Nitrophenyl-phosphate tablets	Sigma-Aldrich	Cat# N2770-5SET
Sodium arsenite solution	Sigma-Aldrich	Cat# 1.06277
4-Thiouridine (4-SU)	Sigma-Aldrich	Cat# T4509
Mepazine acetate	Chembridge	Cat# 5216177
Phorbol- 12-myristate-13-actetate (PMA)	Calbiochem	Cat# 524400
Ionomycin	Calbiochem	Cat# 407950
RIPA lysis buffer, 10x	Merck Chemicals	Cat# 20-188
TRIzol	Thermo Scientific	Cat# 15596026
Imject Alum	Thermo Scientific	Cat# 77161
Halt Phosphatase Inhibitor Cocktail	Thermo Scientific	Cat# 78420
LIVE/DEAD Fixable Blue Dead Cell Stain Kit	Thermo Scientific	Cat# L23105
Rapamycin	LC Laboratories	Cat# LCL-R-5000-50
PI-3065	Tocris Bioscience	Cat# 5919
NP-KLH	Biosearch Technologies	Cat# N-5060
NP-BSA, ratio > 20 (NP30)	Biosearch Technologies	Cat# N-5050H-10
NP-BSA, ratio 1-9 (NP2)	Biosearch Technologies	Cat# N-5050L-10
cOmplete™, EDTA-free Protease Inhibitor Cocktail EASYpacks	Roche	Cat# 04693132001
RNA, 16S- and 23S-ribosomal from *E. coli* MRE600	Roche	Cat# 10206938001
Sheep Red Blood Cells (SRBC)	ACILA AG	N/A

(*Continued on next page*)

Continued

REAGENT or RESOURCE	SOURCE	IDENTIFIER
Recombinant mouse IL-6	Peprotech	Cat# 216-16
Recombinant human TGF-β	R&D Systems	Cat# 240-B002
Recombinant human IL-2 (ProleukinS)	Novartis	Cat# 02238131
Streptavidin-AP	Southern Biotech	Cat# 7100-04
Bio-Rad Protein Assay Dye Reagent Concentrate	Bio-Rad Laboratories	Cat# 5000006
Amersham ECL Prime Western Blotting Detection Reagent	GE Healthcare	Cat# RPN2232
Percoll	GE Healthcare	Cat# 17-0891-01
Vectashield	Vector Laboratories	Cat# H-1000
Hematoxylin	Vector Laboratories	Cat# H-3401
Eosin-Y, alcoholic	J.T. Baker	Cat# 3800
Geneticin (G418)	GIBCO	Cat# 10131035
Blasticitin S HCl	GIBCO	Cat# A1113902
HBSS (1x)	GIBCO	Cat# 14175053
Critical Commercial Assays		
EasySep Mouse $CD4^+$ T cell Isolation Kit	STEMCELL Technologies	Cat# 19852
BioPlex Pro Mouse Cytokine Grp I Panel 23-Plex	Bio-Rad Laboratories	Cat# M60009RDPD
BioPlex Pro Mouse Th17 Panel 7-Plex	Bio-Rad Laboratories	Cat# LJ00000163
MILLIPLEX MAP TGFß Magnetic Bead 3 Plex Kit	Merck Chemicals	Cat# TGFBMAG-64K-03
Wes Separation Module 12-230 kDa	ProteinSimple	Cat# SM-W004
ARTSeq Ribosome Profiling Kit for mammalian cells	Illumina	Cat# RPHMR12126
Ribo-Zero Magnetic Kit (human/mouse/rat)	Illumina	Cat# MRZH11124
Nextera XT DNA Sample Preparation Kit	Illumina	Cat# FC-131-1024 and Cat# FC-131-1001
Encore Complete RNA-Seq DR Multiplex Systems	NuGEN Technologies	Cat# 0333-32 and Cat# 0334-32
SMART-Seq v4 Ultra Low Input RNA Kit	Clontech	Cat# 634889
Click-iT HPG Alexa Fluor 488 Protein Synthesis Assay Kit	Thermo Scientific	Cat# C10428
QuikChange II XL Site-Directed Mutagenesis Kit	Agilent	Cat# 200521
NucleoSpin RNA Kit	Macherey-Nagel	Cat# 740955
DNeasy Blood and Tissue Kit	QIAGEN	Cat# 69504
QuantiTect Rev. Transcription Kit	QIAGEN	Cat# 205311
RNA Clean and Concentrator-5 Kit	Zymo Research	Cat# R1015
Genomic DNA Clean and Concentrator-10 Kit	Zymo Research	Cat# 4010
EZ DNA Methylation-Lightning Kit	Zymo Research	Cat# D5030
TaqMan MicroRNA Reverse Transcription Kit	Applied Biosystems	Cat# 4366596
Deposited Data		
RNA-Seq	This paper	GEO: GSE86110
PAR-CLIP	This paper	GEO: GSE86110
Ribosome Profiling	This paper	GEO: GSE86110
Ribosomal proteins-encoding mRNAs	https://david.ncifcrf.gov	N/A
5′ TOP mRNAs	Thoreen et al., 2012	N/A
Experimental Models: Cell Lines		
HEK293T	ATCC	Cat# CRL-3216; RRID: AB_CVCL_0063
Wild-type Mouse Embryonic Fibroblasts (MEF)	Vogel et al., 2013	N/A
Rc3h1-2$^{-/-}$ MEF	Vogel et al., 2013	N/A
Rc3h1-2$^{fl/fl}$; *Cre-ERT2* MEF	Schlundt et al., 2014	N/A

(*Continued on next page*)

Continued

REAGENT or RESOURCE	SOURCE	IDENTIFIER
Experimental Models: Organisms/Strains		
Mouse: C57BL/6	Charles River Laboratories	RRID: IMSR_JAX:000664
Mouse: *Foxp3-IRES-YFP-Cre*	Chinen et al., 2016	N/A
Mouse: miR-17∼92$^{fl/fl}$	The Jackson Laboratory	RRID: IMSR_JAX:008458
Mouse: *Gt(ROSA)26Sor*$^{tm1(EYFP)Cos}$	The Jackson Laboratory	RRID: IMSR_JAX:006148
Mouse: μMT	The Jackson Laboratory	RRID: IMSR_JAX:002288
Mouse: B6-Ly5.1	Charles River Laboratories	RRID: IMSR_CRL:564
Mouse: *Rag1*$^{-/-}$	Charles River Laboratories	RRID: IMSR_JAX:002216
Mouse: *Rc3h1*$^{fl/fl}$	Vogel et al., 2013	N/A
Mouse: *Rc3h2*$^{fl/fl}$	Vogel et al., 2013	N/A
Mouse: *Cd4-Cre*	Vogel et al., 2013	N/A
Mouse: *Cd4-CreERT2*	Janowski et al., 2016	N/A
Mouse: DEREG	Lahl and Sparwasser, 2011	N/A
Oligonucleotides		
Primer: *Itch* (1-1513) forward 5′-TTG TTT AGA CCT TAA GCC ACC-3′	IDT	N/A
Primer: *Itch* (1-1513) reverse 5′-ATG ACA TGT ATT TCT TGT G-3′	IDT	N/A
Primer: *Itch* (1411-2389) forward 5′-ACT GCC ATC CTC AGC AGA GAC-3′	IDT	N/A
Primer: *Itch* (1411-2389) reverse 5′-TCA CTC CAT TGG ACG AGA G-3′	IDT	N/A
PrimeTime Primer 1: *Pten* 5′-TTCACCTTTAGCTGGCAGAC-3′	IDT	Assay ID: Mm.PT.56a.8966497
PrimeTime Primer 2: *Pten* 5′-CAC TGC TGT TTC ACA AGA TGA TG-3′	IDT	Assay ID: Mm.PT.56a.8966497
PrimeTime Primer 1: *Ywhaz* 5′-AGA ATG AGG CAG ACA AAG GTT-3	IDT	Assay ID: Mm.PT.58.8991239
PrimeTime Primer 2: *Ywhaz* 5′-AGA GTC GTA CAA AGA CAG CAC-3′	IDT	Assay ID: Mm.PT.58.8991239
NEXTflex Small RNA Barcode Primers – Set A	Bioo Scientific	Cat# 513305
mTSDR 5′ biotinylated Primer forward 5′-TAAGGGGGTTTTAATATTTATGAGGTTT-3′	Eurofins Genomics	N/A
mTSDR Primer reverse: 5′-CCTAAACTTAACCAAATTTTTCTACC-3′	Eurofins Genomics	N/A
mTSDR sequencing Primers: S1: ACCCAAATAAAATAATATAAATACT S2: ATCTACCCCACAAATTT S3: AACCAAATTTTTCTACCATT	Eurofins Genomics	N/A
hsa-miR-17 (TaqMan MicroRNA Assay): CAAAGUGCUUACAGUGCAGGUAG	Applied Biosystems	Assay ID: 002308
hsa-miR-19a (TaqMan MicroRNA Assay): UGUGCAAAUCUAUGCAAAACUGA	Applied Biosystems	Assay ID: 000395
snoRNA202 (TaqMan MicroRNA Control Assay): GCTGTACTGACTTGATGAAAGTACTTTTGAAC CCTTTTCCATCTGATG	Applied Biosystems	Assay ID: 001232
Recombinant DNA		
pGEM-T Easy	Promega	Cat# A1360
MSCV-hICOS/GFP-IRES-Thy1.1	Jeltsch et al., 2014; Schlundt et al., 2014	N/A
KMV-hICOS-3′UTR-IRES-GFP	Jeltsch et al., 2014	N/A

(*Continued on next page*)

Continued

REAGENT or RESOURCE	SOURCE	IDENTIFIER
pLenti CMVtight NEO DEST	Addgene	Cat# 26432
pLenti CMV rtTA3 Blast	Addgene	Cat# 26429
Software and Algorithms		
SoftMax Pro 7 Software	Molecular Devices	N/A
BioPlex Manager 6.1 Software	Bio-Rad Laboratories	N/A
IDEAS software	Merck Chemicals	N/A
Compass software for Simple Western	ProteinSimple	N/A
softWoRx 6.0 Beta 19 (Unreleased) Software Suite	GE Healthcare	N/A
Light Cycler 480 SW 1.5.1	Roche	N/A
FlowJo software	TreeStar	RRID: SCR_008520
ImageJ	https://imagej.net	RRID: SCR_003070
FASTX-toolkit	http://hannonlab.cshl.edu/fastx_toolkit/	RRID: SCR_005534
DAVID	https://david.ncifcrf.gov	RRID: SCR_001881
Segemehl Software	Hoffmann et al., 2009; http://www.bioinf.uni-leipzig.de/Software/segemehl/	RRID: SCR_005494
DESeq2	Love et al., 2014; https://bioconductor.org/packages/release/bioc/html/DESeq2.html	RRID: SCR_015687
R package *babel*	Olshen et al., 2013	N/A
Gene Set Enrichment Analysis (GSEA) v2.2.3	http://software.broadinstitute.org/gsea/index.jsp	RRID: SCR_003199
KEGG database	http://www.kegg.jp	RRID: SCR_012773
CLIPZ	Khorshid et al., 2011	RRID: SCR_005755
TargetScan	http://www.targetscan.org/	RRID: SCR_010845
Clustal Omega	https://www.ebi.ac.uk/Tools/msa/clustalo/	RRID: SCR_001591
RNAalifold	http://rna.tbi.univie.ac.at/cgi-bin/RNAWebSuite/RNAalifold.cgi	RRID: SCR_008550
Other		
Collagenase Type IV	Worthington Biochemical Corporation	Cat# LS004188
DNase I	Roche	Cat# 11284932001
Liberase DH	Roche	Cat# 05401089001
Benzonase Nuclease	Merck Chemicals	Cat# 70746
Calf Intestinal Phosphatase (CIP)	NEB	Cat# M0290S
Q5 High-Fidelity 2x Master Mix	NEB	Cat# M0492S

CONTACT FOR REAGENT AND RESOURCE SHARING

Further information and requests for resources and reagents should be directed to and will be fulfilled by Vigo Heissmeyer (vigo.heissmeyer@med.uni-muenchen.de) or Desheng Hu (desheng_hu@126.com).

EXPERIMENTAL MODEL AND SUBJECT DETAILS

Mice

All animals were housed in a pathogen-free barrier facility in accordance with the Helmholtz Zentrum München and the Ludwig-Maximilians-Universität München institutional, state and federal guidelines. All experimental procedures involving mice were performed in accordance with the regulations of and were approved by the local government (Regierung von Oberbayern).

METHOD DETAILS

Immunization with NP-KLH

Mice were immunized i.p. with 100 μL of 0.5 mg/ml NP-KLH in combination with Imject Alum as adjuvant. On day 7 mice were sacrificed and splenic Tfh and GC B cells were analyzed by flow cytometry. In a further experiment serum samples of the immunized mice were collected once a week. After four weeks mice were sacrificed and the sera of each time point were analyzed for NP-specific antibodies by ELISA.

ELISA

ELISA was performed as previously described (Baumjohann et al., 2013b). Briefly, Nunc MaxiSorp 96-well plates (Invitrogen) were coated with 5 μg/ml goat anti-mouse Ig antibodies (IgG, IgG1 or IgGM) or 10 μg/ml NP30/NP2-BSA at 4°C overnight. Plates were blocked with 2% BSA in PBS and serum samples or standards (mouse IgG, IgG1 or IgM) diluted in 1% BSA in PBS were added. Alkaline Phosphatase (AP)-conjugated goat anti-mouse Ig isotype-specific antibodies (IgG and IgG1) were used as detection antibodies. For the measurement of IgM levels a biotinylated detection antibody was used followed by AP-conjugated streptavidin. Plates were read at 405nm using the VersaMax ELISA Microplate Reader (Molecular Devices), analyzed with Soft Max Pro 7 software, and curves were fitted using a 4 - parameter - logistic fit.

In vivo colitis model

Eight weeks old, female *Rag1*$^{-/-}$ mice were injected i.p. with 2 x10^5 CD45.1$^+$CD4$^+$CD25$^+$CD62L$^+$CD44$^-$ naive T cells sorted from Ly5.1 mice or with these naive T cells mixed with 1 x10^5 CD45.2$^+$CD4$^+$YFP$^+$ Treg cells from either WT or DKO^{Treg} mice.

Histology

4% paraformaldehyde-fixed paraffin-embedded colon sections (3 μm) were stained with hematoxylin/eosin (H&E). Colitis was quantified using a histological score in a blinded fashion by two independent investigators. Slides were scored for leucocyte infiltration, epithelial damage, goblet cell loss and hyperplasia (each scaled from 0-3, resulting in a maximal score of 12).

Cell Culture of MEF and T cells

MEF cells were cultured in Dulbecco's Modified Eagle's Medium (DMEM) (GIBCO) supplemented with 10% (v/v) fetal bovine serum (FBS) (PAN-Biotech), 1,000 U/ml penicillin-streptomycin (GIBCO), and 10 mM HEPES, pH 7.4 (GIBCO) at 37°C in 10% CO_2.

T cells were cultured in DMEM medium supplemented with 10% (v/v) FBS (PAN Biotech), 1x non-essential amino acids (Lonza), 10 mM HEPES, pH7.4 (GIBCO), 50 μM β-mercaptoethanol (GIBCO) and 1,000 U/ml penicillin-streptomycin (GIBCO) at 37°C in 5% CO_2.

In vitro and *in vivo* deletion of Roquin-1 and Roquin-2 encoding genes and inhibition of MALT1

For *in vitro* deletion of Roquin-1 and Roquin-2 encoding genes in MEF cells, *Rc3h1-2*$^{fl/fl}$*; Cre-ERT2* MEF cells were treated with 0.3 μM of 4' OH-tamoxifen for 5 d before analysis. For *in vitro* deletion in T cells, total CD4$^+$ T cells from *Rc3h1-2*$^{fl/fl}$; *Cd4-Cre-ERT2* mice were isolated from spleen and lymph nodes using the EasySep^{TM} Mouse CD4$^+$ T cell Isolation Kit and treated with 1 μM 4' OH-tamoxifen for 24 hr. CD4$^+$ T cells were washed twice with medium to remove 4' OH-tamoxifen and stimulated with anti-CD3 (0.5 μg/mL) and anti-CD28 (2.5 μg/mL) on six-well plates pre-coated with goat-anti-hamster IgG (0.05 mg/mL in PBS overnight at 4°C) for 48 hr at an initial cell density of 1 × 10^6 cells/mL. After stimulation, cells were expanded in media with 200 U/ml of recombinant human IL-2 for 48 hr. For *in vivo* deletion *Rc3h1-2*$^{fl/fl}$; *Cd4-Cre-ERT2* mice were gavaged with 5 mg tamoxifen in 150 μL corn oil per mouse daily for 4 d. The mice were sacrificed on day 5 for analysis. For MALT1 inhibition, purified WT CD4$^+$ T cells were pre-incubated with mepazine (20 μM) or dimethyl sulfoxide (DMSO) (1:2500) for 3 hr and then stimulated with PMA (20 nM) and ionomycin (1 μM) for 60 min.

Rapamycin treament of iDKO^T mice

For *in vivo* deletion of Roquin-1 and Roquin-2 encoding genes, *Rc3h1-2*$^{fl/fl}$; *Cd4-Cre-ERT2* mice were gavaged with 5 mg tamoxifen in corn oil per mouse for 4 days. After the first tamoxifen treatment mice were injected i.p. with 4 mg/kg rapamycin (dissolved in 5% Tween-80 and 5% PEG-400 in PBS) or a vehicle control (5% Tween-80 and 5% PEG-400 in PBS) every two days. Mice were sacrificed and analyzed on day 8.

Adoptive transfer experiments

Rapamycin-sensitivity of Tfh cell differentiation was examined in μMT mice. μMT mice were given adoptive cell transfer of CD4$^+$ T cells from *Rc3h1-2*$^{fl/fl}$*; Gt(ROSA)26Sor*$^{tm1(EYFP)Cos}$*; Cd4-Cre-ERT2*. CD4$^+$ T cells were depleted for B cells by the addition of a biotinylated anti-B220 antibody to the EasySep^{TM} Mouse CD4$^+$ T cell Isolation Kit. CD4$^+$ T cells (10 x10^6) were transferred into μMT hosts via i.v. injection one day prior to immunization. Deletion of Roquin-1 and Roquin-2 encoding genes was induced by tamoxifen gavage on days 0, 1, 2, 3. Immunization was done by i.v. injection of 1 x10^8 sheep erythrocytes (SRBCs) on day 0 and mice were treated with rapamycin or vehicle i.p. on days −1, 1, 3, 5, 7. Mice were sacrificed and analyzed on day 8.

In vitro T cell differentiation with different PI3K-mTOR inhibitors

In vitro T cell differentiation was conducted by culturing sorted naive $CD4^+CD44^{lo}CD62L^{hi}$ T cells in anti-CD3 (2 μg/ml) and anti-CD28 (2 μg/ml) coated 96-well plates under the following conditions: Th17, TGF-β (2.5 ng/ml), IL-6 (25 ng/ml), anti-IL-4 (10 μg/ml) and anti-IFN-γ (10 μg/ml); and Treg, TGF-β (1 ng/ml), anti-IL-4 (10 μg/ml) and anti-IFN-γ (10 μg/ml). Th17 and Treg cells were cultured for 3.5 d. Rapamycin was used at concentrations of 0.1, 1.0 and 10 nM, LY294002 was used at concentrations of 10, 50 and 3000 nM and PI-3065 was used at concentrations of 0.1, 0.5 and 1 μM.

Flow cytometry and cell sorting

Single-cell suspensions were pre-incubated with Fc-block (CD16/32) in staining buffer (PBS with 2% FBS and 2 mM EDTA) for 10 min at 4°C, and then stained with fixable viability dye for 20 min at 4°C. For the detection of surface markers cells were regularly stained with the appropriate antibodies for 30 min at 4°C, except for the surface marker CCR7, cells were stained with the antibody for 30 min at 37°C. If needed, cells were then fixed and permeabilized for intracellular staining. To stain transcriptional factors such as Foxp3, Bcl-6 and c-Maf as well as the nuclear protein Ki-67, cells were fixed and permeabilized by using the Foxp3 / Transcription Factor Staining buffer set according to manufacturer's instructions. To maintain the YFP signal before intracellular staining samples were pre-fixed in 1% paraformaldehyde in PBS for 15 min at room temperature. For intracellular cytokine staining, $CD4^+$ T cells were stimulated with PMA (20 nM) and ionomycin (1 μM) for 4 hr and brefeldin A (5 μg/ml) was added for the last 2 hr before being stained according to the manufacture's instructions (eBioscience). For staining of phospho-S6, cells were fixed in 2% formaldehyde for 15 min at room temperature and permeabilized in 0.5% saponin buffer for 20 min at 4°C. For staining of phospho-Akt Ser473 and phospho-Akt Thr308, cells were fixed with IC Fixation Buffer for 10 min at room temperature, and permeabilized in ice-cold 90% methanol for 30 min on ice. Then cells were stained with the appropriate antibodies in staining buffer for 30-60 min (P-S6 and P-Akt Ser473) or overnight (P-Akt Thr308) at 4°C. To detect the phospho-S6 antibody a secondary goat-anti-rabbit Alex647 antibody was applied. For staining of Pten, cells were fixed with Cytofix Fixation Buffer for 10 min at 37°C and subsequent permeabilization in Phosflow Perm Buffer III for 30 min at 4°C. Then cells were stained for Pten (A2B1) in staining buffer for 30 min at 4°C. For staining of Glut-1 cells were fixed with 4% paraformaldehyde for 15 min at room temperature and then stained with the appropriate antibody for 1 h at room temperature. For detection of Glut-1 a secondary goat-anti-rabbit Alex647 was applied. After staining, cells were acquired on a FACS Fortessa (BD Biosciences), FACS Canto II (BD Biosciences) or Cytoflex (Beckman Coulter) device and samples were analyzed with FlowJo software.

For staining of Foxo1, cells were fixed with 2% formaldehyde in PBS for 20 min at 4°C, and permeabilized in PBS containing 0.1% Triton X-100 and 1% BSA, cells were stained with purified Foxo1 antibody for 30 min at 4°C followed by a second antibody staining using goat-αnti−rabbit FITC. Finally, the cells were stained with DRAQ5 and measured with the Amnis ImageStream (Millipore). Similarity score between Foxo1 and DRAQ5 was calculated using the IDEAS software similarity feature.

For cell sorting, samples were first stained with surface antibodies and sorted on a FACSAria Fusion cell sorter (BD).

In vitro suppression assay

YFP^-CD4^+ (responder) T cells were sorted from WT (*Foxp3-cre*) mice and labeled with the cell proliferation dye eF450 (CPD450) to culture them alone or with sorted $CD4^+YFP^+$ Treg cells from WT (*Foxp3-cre*) or DKO^{Treg} mice under anti-CD3 (0.1 μg/ml) stimulation and in the presence of $1x10^5$ irradiated splenocytes per well in a 96-well round bottom plate. 2.5×10^4 responder cells were mixed with YFP^+ Treg cells in 1:1, 2:1, and 4:1 ratios. After 72 hr, cultured cells were harvested and assessed for the proliferation of the responder cells based on the dilution of fluorescence intensity of CPD450.

Lamina propria lymphocyte isolation and staining

Mice were sacrificed, colons were removed and flushed with ice cold PBS. Colons were cut into small pieces, pre-digested in HBSS supplemented with 8% FCS, 10 mM HEPES, 10 mM EDTA followed by three digestions in HBSS supplemented with 8% FCS, Collagenase Type IV (157 U/ml), DNase I (0.2 mg/ml) and Liberase DH (0.125 mg/ml). Lymphocytes were purified using a 40/80 Percoll gradient. Purified lymphocytes were stained with LIVE/DEAD fixable blue followed by surface staining and intracellular staining.

Multiplex cytokine/chemokine analysis

Sorted YFP^+ and YFP^- Treg cells were *ex vivo* stimulated with anti-CD3/anti-CD28 (plate-coated, 2 μg/ml). After 48 hr cell supernatants were harvested and analyzed by Bio-Plex assay.

Cytokines and chemokines in serum and cell supernatants were measured using multiplex bead array systems, Bio-Plex Pro Mouse Cytokine Grp I Panel 23-Plex, Bio-Plex Pro Mouse Th17 Panel 7-Plex, and MILLIPLEX® MAP TGF-β Magnetic Bead Panel, following the manufacturers' recommendations. TGFβ in serum and supernatants was converted into its active form by acidification before analysis. Data were acquired using the Luminex100 machine with BioPlex Manager 6.1 software. Standard curves were fitted using the logistic-5PL regression type.

The minimal detectable concentrations (listed in brackets) were:

Bio-Plex Pro Mouse Th17 Panel 7-Plex: MIP-3a (18 pg/ml), IL-33 (1.3 pg/ml), IL-31 (6.5 pg/ml), IL-23p19 (7 pg/ml), IL-22 (1 pg/ml), IL-21 (7 pg/ml), IL-17F (3 pg/ml); Bio-Plex Pro Mouse Cytokine Grp I Panel 23-Plex: IL-1a (0.8 pg/ml), IL-1β (1.8 pg/ml), IL-2 (2.6 pg/ml), IL-3 (1.1 pg/ml), IL-4 (3.5 pg/ml), IL-5 (1.3 pg/ml), IL-6 (0.9 pg/ml), IL-9 (2.5 pg/ml), IL-10 (2.9 pg/ml), IL-12p40 (1.4 pg/ml), IL-12p70 (2 pg/ml), IL-13 (3.5 pg/ml), IL-17 (2.5 pg/ml), Eotaxin (2.5 pg/ml), G-CSF (2.2 pg/ml), GM-CSF (6.2 pg/ml),

IFN-γ (1.2 pg/ml), KC (1.8 pg/ml), MCP-1 (7.5 pg/ml), MIP-1a (0.9 pg/ml), MIP-1β (2 pg/ml), RANTES (0.7 pg/ml), TNF-α (3.6 pg/ml); EMD MILLIPLEX® MAP TGF-β1, - β2 and - β3 Magnetic Bead Panel detects the active TGFβ, with minimal detectable concentrations of 9.8 pg/ml for TGF-β1, 2.6 pg/ml for TGF-β2 and 2.2 pg/ml for TGF-β3.

Immunoblot analysis

For protein extraction from $CD4^+$ T cells or MEF cells, these were washed twice with ice-cold 1x PBS and lysed in 20 mM Tris-HCl, pH 7.5, 150 mM NaCl, 0.25% (v/v) Nonidet-P40, 1.5 mM $MgCl_2$, 1 mM DTT supplemented with 1x cOmplete, EDTA-free Protease Inhibitor Cocktail and 1x Halt Phosphatase Inhibitor Cocktail on ice for 15 min. Lysates were cleared by centrifugation at 12.000 xg for 15 min at 4°C and the protein concentration was measured by a Bio-Rad Protein assay. Equal amounts of total protein (10-50 μg) were separated by SDS-PAGE, transferred to a nitrocellulose membrane and analyzed by using primary antibodies followed by horseradish peroxidase (HRP)-conjugated secondary antibodies. For protein detection, the Amersham ECL Prime Western Blotting Detection Reagent and X-ray films were used.

Automated capillary electrophoresis western analysis

Sorted GFP^+ Treg cells (500.000 cells) from DEREG mice (Lahl and Sparwasser, 2011) were lysed in 25 μL of 1x RIPA lysis buffer supplemented with 1x cOmplete, EDTA-free Protease Inhibitor Cocktail, 1x Halt Phosphatase Inhibitor Cocktail, 0.1% SDS and 2.5 U Benzonase Nuclease. A total of 3 μL of the sample, a mixture of lysate and 1x Fluorescent Master Mix, was loaded into plates and capillary electrophoresis Western analysis was carried out following the manufacturer's instructions (see Wes Separation Module 12-230 kDa, ProteinSimple). The primary antibodies against Itch and Pten (D4.3) were incubated for 90 min. The data were analyzed with the Compass software.

Immunofluorescence

Mice were immunized with 60-100 × 10^6 SRBCs i.v. After 7 days mice were sacrificed and spleens were frozen in OCT (Tissue Tek). Then cryosections (6 μm) were prepared and fixed in aceton. Slides were stained with CD4-FITC (GK1.5), Foxp3-Biotin (FJK) and Streptavidin-AlexaFluor555 and GL-7-Alexa647. Images were acquired on an Olympus BX41 fluorescence microscope. To determine the size of germinal centers (GC), a region of interest (ROI) was drawn around the $GL\text{-}7^+$ area and its size measured using ImageJ. To determine the number of Tfr cells, $CD4^+Foxp3^+$ were counted within the GC ROI.

3D SIM

Rc3h1-2$^{-/-}$ MEF cells that contained a doxycycline-inducible cassette for re-expression of Roquin-1 or different Roquin mutants were seeded onto coverslips and treated with 1 μg/ml of doxycycline for 14 hr. Before fixation, cells were treated with 0.5 mM sodium arsenite for 1 hr at 37°C or left untreated. Cells were fixed with 2% formalin in PBS for 10 min and then permeabilized in PBS containing 0.02% Tween20 and 0.5% Triton X-100 for 10 min. Coverslips were treated with the MAXblock Blocking Medium (Active Motif) for 2 hr at room temperature. Subsequently, cells were stained with the primary antibodies against Roquin (18F8) and either p70 S6 kinase α (H-9) or G3BP1 followed by a second antibody staining using anti-rat Alexa Fluor 488, anti-mouse CF405S or anti-rabbit Alexa Fluor 594. After a final fixation step in 4% formalin in PBS the cells were mounted in Vectashield. Images were acquired with a DeltaVision OMX V3 microscope. 3D SIM raw data were first reconstructed with the software softWoRx 6.0 Beta 19 (Unreleased) and corrected for color shifts. Composite TIFF stacks were established.

Ribosome profiling

Ribosome profile was carried out with the ARTseq Ribosome Profiling Kit for mammalian cells, according to the manufacturer's instructions. MEF cells (4-5 × 10^7) or $CD4^+$ T cells (5-6 × 10^7) were washed with pre-warmed medium containing 100 μg/ml of cycloheximide for 1 min. MEF cells were lysed in 800 μl and T cells in 400 μl lysis buffer (1x Polysome Buffer, 1% Triton X-100, 1 mM DTT, 25 U/ml DNase I and 100 μg/ml of cycloheximide). After clarification of the lysates for 10 min at 20.000 x g at 4°C cell extracts were treated with 20-30 units of ARTSeq Nuclease (10 U/μl) at room temperature for 45 min with gentle mixing. Nuclease was inactivated with 10 μl of SUPERase●In RNase Inhibitor. The 80S monosomes were purified by size-exclusion chromatography using MicroSpin S-400 HR columns (GE Healthcare), according to the manufacturer's instructions. After equilibration of the columns with 1x Polysome Buffer, 100 μL of RNase digested cell extracts were applied to each column. In total two MicroSpin S-400 HR columns were used for each sample. The 80S monosomes together with other large proteins or protein complexes were eluted by centrifugation for 2 min at 600 x g. The columns were washed with 100 μl of 1x Polysome Buffer (1 min/735 x g). The eluates belonging to the same samples (200 μL in total) were pooled and RNA was extracted with acid phenol:chloroform:isoamyl alcohol (125:24:1, pH 4.5). RNA was precipitated with ethanol and rRNA was depleted with the Ribo-Zero Magnetic Kit (Human/Mouse/Rat). The procedure was performed according to the manufacturer's manual, with the exception of the 50°C incubation step. RNA was analyzed on a 15% urea polyacrylamide gel, ribosome-protected fragments (RPFs) of 28-30 nt were excised, and then eluted from the gel overnight in 300 mM NaCl, followed by ethanol precipitation. For the generation of the cDNA library RPFs were 3'-dephosphorylated, ligated with a 3' adaptor, reverse transcribed, circularized and finally PCR amplified according to the ARTseq Ribosome Profiling Kit. PCR products were separated on a non-denaturing 8% polyacyrlamide TBE gel and DNA fragments of the correct size (nt 113 + 28-30) were extracted. cDNA libraries were sequenced using an Illumina HighSeq2000 sequencer.

RNA input for sequencing

Total RNA from sorted $CD4^+YFP^+GITR^+CD25^+$ and $CD4^+YFP^+GITR^+CD25^-$ cells was extracted using TRIzol according to the manufacturer's instructions and cDNA libraries were performed using the Encore Complete RNA-Seq DR Multiplex Systems.

Total RNA for Ribosome profiling analysis was purified from 200 μL of clarified MEF cell lysate without ARTseq Nuclease treatment using acid phenol:chloroform:isoamyl alcohol (125:24:1, pH 4.5), followed by ethanol precipitation. cDNA libraries were performed with 100 ng of total RNA using the Encore Complete RNA-Seq DR Multiplex Systems. Total RNA from 6 $x10^6$ T cells was extracted using TRIzol according to the manufacturer's instructions. cDNA libraries were generated from 10 ng of total RNA using the SMART-Seq v4 Ultra Low Input RNA Kit for Sequencing and Nextera XT DNA Sample Preparation Kit. cDNA libraries were sequenced using an Illumina HighSeq 2000 or HighSeq 1500 sequencer.

PAR-CLIP

The method was performed as described in (Hafner et al., 2010). In brief, WT MEF cells overexpressing Roquin-1 were labeled with 100 μM 4-Thiouridine (4-SU) for 16 hr. After irradiation of the cells using UV light at 365 nm, cells were lysed in NP40 lysis buffer (50 mM HEPES-KOH at pH 7.4, 150 mM KCl, 2 mM EDTA, 0.5% (v/v) NP40, 0.5 mM DTT, and 1x cOmplete, EDTA-free Protease Inhibitor Cocktail). Immunoprecipitation was carried out with Dynabeads protein G coupled to Roquin antibody (3F12) for 2 hr at 4°C. Beads were treated with calf intestinal phosphatase (CIP) and RNA fragments were radioactively end labeled. The crosslinked protein-RNA complexes were purified on 4%–12% NuPAGE gel (Invitrogen), and the 125 kDa band corresponding to Roquin was cut out. The RNA was isolated by electroelution followed by Proteinase K digestion and phenol-chloroform extraction. cDNA library was prepared according to the standard small RNA protocol (Hafner et al., 2012) with a minor modification. For PCR amplification the NEXTflex small RNA barcode primers were used. The amplified cDNA was sequenced on an Illumina HighSeq2000 sequencer.

Click-iT nascent protein synthesis assay

Protein biosynthesis was detected by the Click-iT HPG Alexa Fluor Protein synthesis Assay Kit. MEF cells were seeded at a density of 2-3 × 10^5 per well of a 6-well plate. After 16 hr, cells were washed with warm PBS and methionine-free DMEM medium (GIBCO) supplemented with 50 μM of Click-iT L-homopropargylglycine (HPG) was added. After incubation at 37°C for 6-8 hr, cells were trypsinized and transferred into a 96 U-bottom well plate. Cells were fixed with 2% of formaldehyde at room temperature for 15 min, followed by permeabilization in PBS supplemented with 0.5% saponin and 1% BSA at 4°C for 20 min. HPG was detected using the Click-iT reaction cocktail containing Alexa Fluor 488 azide according to the manufacturer's instructions.

Cloning and analysis of the Itch 3' UTR reporter constructs

The 3' UTR sequences of *Itch* (1-1513 and 1411-2389) were amplified from mouse genomic DNA using the Q5 High-Fidelity 2x Master Mix with the corresponding primers containing ClaI and SfiI sites at the fragment ends. The PCR-amplified 3' UTR fragments were ligated into the pGEM-T Easy vector, then excised as a ClaI/SfiI fragment and cloned into the MSCV-hICOS/GFP-IRES-Thy1.1 expression vector (Jeltsch et al., 2014; Schlundt et al., 2014). The 3' UTR reporter constructs were analyzed by the infection marker Thy1.1 and GFP and subsequent flow cytometry.

Transfection and viral transduction

Replication-deficient retrovirus production and retroviral infection of MEF cells with the 3' UTR reporter constructs were performed as previously described (Glasmacher et al., 2010; Janowski et al., 2016; Schlundt et al., 2014; Vogel et al., 2013). For lentivirus production, HEK293T cells were seeded to a density of 15 × 10^6 cells in 15 cm culture dishes. Twenty four hours later, transfection was carried out using the calcium phosphate method to introduce packaging and lentiviral plasmids into HEK293T cells. As lentiviral vectors the plentiCMVtight containing either WT Roquin-1 or different Roquin mutants (Roquin (aa1-510), A-site (K220A K239A R260A), Znf (C419R), and RING (C14A)) and the plenti CMV rtTA3 vector were used. plentiCMVtight Neo DEST and the rtTA3-encoding vector plenti CMV rtTA3 Blast was a gift from Dr. Eric Campeau. *Rc3h1-2*$^{-/-}$ MEF cells were cotransduced with plentiCMVtight Roquin-1 or Roquin mutants and the reverse tetracycline-controlled transactivator (rtTA3). Two days after infection, cells were cultured in medium supplemented with 500 μg/ml Geneticin (Neomycin) and 2.85 μg/ml Blasticitin S HCl for 7 d to select for stably infected cells. Roquin-1 mutations were introduced by QuikChange mutagenesis (QuikChange II XL site-directed mutagenesis Kit). Before analysis, cells were treated with 1 μg/ml doxycycline for 14 hr to induce Roquin expression or left untreated.

Coimmunoprecipitation of Roquin-associated mRNAs

Roquin immunoprecipitations were performed as previously described (Glasmacher et al., 2010). Briefly, MEF cells were lysed in 700 μl lysis buffer (20 mM Tris-HCl, pH 7.5, 150 mM NaCl, 0.25% (v/v) Nonidet-P40, 1.5 mM $MgCl_2$, 1 mM DTT supplemented with 1x cOmplete, EDTA-free Protease Inhibitor Cocktail and 1x Halt Phosphatase Inhibitor Cocktail) on ice for 15 min. Lysates were cleared by centrifugation 10 min at 10.000x g. Anti-Roquin-1 (Bethyl Laboratories) or normal IgG bound to protein G magnetic beads was incubated for 4 h at 4°C with lysates. Beads were washed two times with RNA wash buffer (lysis buffer containing 300 mM NaCl, 0.5% (vol/vol) Nonidet-P40 and 2.5 mM MgCl2) and two times with lysis buffer. Beads were split into a small fraction for Western Blot analysis and a large fraction for RT-qPCR analysis. For Western Blot analysis beads were resuspended in 15 μl of 1x SDS loading buffer and the immunoprecipitates were eluted from the beads by heating at 95°C for 5 min. For RNA extraction, 350 μL RA1 buffer (NucleoSpin RNA Kit) supplemented with 10 mM DTT and 4 μg bacterial rRNA (Roche) was added to the beads and to 200 μg of

lysate protein as input samples. The RNA was subsequently extracted using the NucleoSpin RNA Kit according the manufacturer's instructions. For quantification of *Pten, Itch* and *Nfkbiz* mRNA in Roquin immunoprecipitates, RT-qPCR was performed using 1 μg of input RNA and 30 - 40% of immunoprecipitated RNA for cDNA synthesis.

Ago2 immunoprecipitation

Monoclonal antibody for mouse Ago2 (6F4) were coupled to 100 μl of Dynabeads protein G at room temperature for 1 hr. Antibody-conjugated beads were washed twice with citrate-phosphate buffer pH 5.0. $CD4^+$ T cells were isolated from spleen and lymph nodes from *Cd4-Cre-ERT2*, *Rc3h1-2*$^{fl/fl}$; *Cd4-Cre-ERT2*, WT and *miR-17∼92*$^{fl/fl}$; *Cd4-Cre*$^+$ mice. $CD4^+$ T cells from *Cd4-Cre-ERT2* and *Rc3h1-2*$^{fl/fl}$ *Cd4-Cre-ERT2* mice were additionally treated with 1 μM 4' OH-tamoxifen for 24 hr. T cells from each mouse were then activated with anti-CD3 and anti-CD28 for 48 hr and expanded with IL-2 for 48 hr. Cells were washed with ice-cold PBS and T cells (1×10^8) were lysed on ice in 1 mL of lysis buffer (25 mM Tris–HCl pH 7.4, 150 mM KCl, 0.5% (v/v) NP-40, 2 mM EDTA, 1 mM NaF, 0.5 mM DTT and 1x cOmplete EDTA-free Protease Inhibitor Cocktail). The lysates were cleared by centrifugation at 12.000 xg for 15 min at 4°C. The antibody-conjugated magnetic beads were added to 5 mg of total lysate protein and incubated on a rotating wheel overnight at 4°C. Beads were washed once with lysis buffer, two times with IP-wash buffer (50mM Tris–HCl pH 7.4, 300 mM KCl, 1 mM $MgCl_2$, 0.1% (v/v) NP-40, 0.5 mM DTT and 1x cOmplete EDTA-free Protease Inhibitor Cocktail) and once with PBS. Beads were split into a small fraction for Western Blot analysis and a large fraction for RT-qPCR analysis. For Western Blot analysis beads were resuspended in 20 μl of 1x SDS loading buffer and the immunoprecipitates were eluted from the beads by heating at 95°C for 5 min. For RNA extraction, 1 mL TRIzol was added to the beads and to 50 μg of lysate protein as input samples. The RNA was subsequently extracted according the manufacturer's instructions and the RNA was purified using the RNA Clean and Concentrator-5 Kit. For quantification of *Pten* mRNA in Ago2 immunoprecipitates RT-qPCR was performed using 1 μg of input RNA and 60 – 80% of immunoprecipitated RNA for cDNA synthesis.

Genomic DNA isolation and bisulfite pyrosequencing

Genomic DNA (gDNA) was isolated from FACS-purified $CD25^-YFP^+$ and $CD25^+YFP^+$ Treg cells from spleen or thymus using DNeasy Blood & Tissue kit. Next, gDNA was concentrated using Genomic DNA Clean & Concentrator-10 and bisulfite-converted using the EZ DNA Methylation Lightning Kit according to the manufacturer's instructions. Pyrosequencing was performed as described previously (Yang et al., 2016a). Amplification of the Treg cell-specific demethylated region (TSDR) was performed with the biotinylated forward primer mTSDR-for and the reverse primer mTSDR-rev. Sequencing was conducted with the TSDR sequencing primers mTSDR-S1, mTSDR-S2, mTSDR-S3 covering CpG motifs of the TSDR between chromosome position X:7583950-7584149 (genome assembly: GRCm38.p5). Male mice were used for DNA methylation analysis to avoid artificial recalculation due to X chromosome inactivation in female mice.

Quantitative RT-PCR analysis

RT-qPCR was used to quantitate *Pten* expression in $CD4^+$ T cells and *Pten*, *Itch* and *Nfkbiz* expression in immunoprecipitates. RNA was isolated with TRIzol or with the NucleoSpin RNA Kit. cDNA (from 500 ng - 1 μg RNA) was synthesized using the QuantiTect Reverse Transcription Kit according to the manufacturer's instructions. qRT-PCR for *Pten*, *Itch*, and *Ywhaz* was performed using the IDT PrimeTime qPCR Assay consisting of two primers and a hydrolysis probe (5'-FAM/ZEN/IBFQ). qRT-PCR for *Nfkbiz* was performed using Light Cycler 480 Probes Master Mix and primer-/probe-combinations from Roches Universal Probe Library. PCR reactions were run on a Roche Light Cycler 480II machine. Relative gene expression was determined with the Light Cycler 480 SW 1.5.1 software, and normalized to the expression of the housekeeping gene *Ywhaz* or the IgG control.

For measurements of miR-17 and miR-19a, sorted naive ($CD4^+CD62L^+CD44^-$) and effector ($CD4^+CD62L^+CD44^+$) T cells were used. Total RNA, including microRNAs, was extracted with TRIzol and miRNA-specific cDNA was prepared from 15 ng total RNA using the TaqMan MicroRNA Reverse Transcription Kit. The expression of miR-17 and miR-19a was measured by qRT-PCR using the hsa-miR-17, hsa-miR-19a, snoRNA202 Taqman microRNA Assay (Applied Biosystems) on a Light Cycler 480II device with the Light Cycler 480 SW 1.5.1 software.

To determine deletion of Roquin-1 and Roquin-2 encoding alleles, gDNA was isolated using DNeasy Blood & Tissue kit, qRT-PCR for *Rc3h1*, *Rc3h2*, and *Pbdg* were performed using Light Cycler 480 Probes Master Mix and primer-/probe-combinations from Roches Universal Probe Library.

QUANTIFICATION AND STATISTICAL ANALYSIS

Cellular analyses

Statistical analysis was performed with Prism 5.0b (GraphPad). *P* values were calculated with Student's *t test*, one-way or two-way ANOVA. $p < 0.05$ was considered significant. All error bars represent mean and SEM.

mRNA-seq and ribosome profiling differential expression analyses

mRNA-seq reads were first subject 3' adaptor trimming (AGATCGGAAGAGCGGTT) and quality control using the FASTX-toolkit (http://hannonlab.cshl.edu/fastx_toolkit/). Reads were then mapped to the mouse transcriptome based on genome assembly mm10 and transcript annotations from RefSeq with the segemehl software (Hoffmann et al., 2009), v0.1.7-411, allowing with a

minimum mapping accuracy of 90%. Finally, transcript counts were calculated based on uniquely mapped reads and used to estimate differential expression with DESeq2 (Love et al., 2014).

For ribosome profiling, the procedure was similar to the one used above with only two alterations: (1) the 3′ adaptor was different (AGATCGGAAGAGCACACGTCT); (2) only the reads mapped to the gene's coding sequence were counted toward differential expression analysis.

Translation efficiency (TE) fold-change was calculated as the ratio of ribosome protected fragments (RPF) fold-change to mRNA fold-change, and the associated significance was evaluated using the R package *babel* (Olshen et al., 2013).

Gene set enrichment analysis

The tool GSEA v2.2.3 (http://software.broadinstitute.org/gsea/index.jsp) was used to calculate the enrichment of different pathways described in the KEGG database (http://www.kegg.jp).

Gene annotations

Ribosomal proteins-encoding mRNAs were retrieved from DAVID (https://david.ncifcrf.gov), 5′ TOP mRNAs as defined in ref. (Thoreen et al., 2012).

PAR-CLIP analysis and identification of the RNA secondary structure in the *Pten* mRNA

We used CLIPZ (Khorshid et al., 2011) to identify Roquin-bound clusters in mouse transcripts based on the fold enrichment of PAR-CLIP reads over mRNA-seq reads. The enrichment is expressed as r_i / ($p_i r$), where r_i is the number of CLIP reads associated with site i, r is the total number of CLIP reads and p_i is the relative abundance of the mRNA in which site i resides. Only clusters containing more than 50 CLIP reads were considered.

To identify an evolutionarily conserved RNA secondary structure in the *Pten* mRNA, we have first collected the mRNA sequences around the TargetScan-predicted miR-17∼92 binding site from seventeen different vertebrate species (http://www.targetscan.org/), and then used Clustal Omega (https://www.ebi.ac.uk/Tools/msa/clustalo/) to perform the multiple alignment of the different sequences and RNAalifold (http://rna.tbi.univie.ac.at/cgi-bin/RNAWebSuite/RNAalifold.cgi) to find the consensus secondary structure.

DATA AND SOFTWARE AVAILABILITY

The accession number for the sequencing data used for analysis in this paper is GEO: GSE86110.